1521-0103/384/3/382–392$35.00
THE JOURNAL OF PHARMACOLOGY AND EXPERIMENTAL THERAPEUTICS

dx.doi.org/10.1124/jpet.122.001423
J Pharmacol Exp Ther 384:382–392, March 2023

The Journal of PHARMACOLOGY And Experimental Therapeutics

The Novel, Clinical-Stage Soluble Guanylate Cyclase Activator BI 685509 Protects from Disease Progression in Models of Renal Injury and Disease[S]

Glenn A. Reinhart, Paul C. Harrison, Kathleen Lincoln, Hongxing Chen, Peng Sun, Jon Hill, Hu Sheng Qian, Mark C. McHugh, Holly Clifford, Khing Jow Ng, Hong Wang, Danielle Fowler, Kristina Gueneva-Boucheva, Jehrod B. Brenneman, Todd Bosanac, Diane Wong, Ryan M. Fryer, Chris Sarko, Carine M. Boustany-Kari, and Steven S. Pullen

Departments of Cardiometabolic Diseases Research (G.A.R., P.C.H., K.L., H.C., P.S., H.S.Q., M.C.M., H.C., K.J.N., H.W., D.F., R.M.F., C.M.B.-K., S.S.P.), Small Molecule Discovery Research (K.G.-B., J.B.B., T.B., D.W., C.S.), and Global Computational Biology and Data Sciences (J.H.), Boehringer Ingelheim Pharmaceuticals, Inc, Ridgefield, Connecticut

Received August 23, 2022; accepted November 28, 2022

ABSTRACT

Activation of soluble guanylate cyclase (sGC) to restore cyclic guanosine monophosphate (cGMP) and improve functionality of nitric oxide (NO) pathways impaired by oxidative stress is a potential treatment of diabetic and chronic kidney disease. We report the pharmacology of BI 685509, a novel, orally active small molecule sGC activator with disease-modifying potential. BI 685509 and human sGC $\alpha1/\beta1$ heterodimer containing a reduced heme group produced concentration-dependent increases in cGMP that were elevated modestly by NO, whereas heme-free sGC and BI 685509 greatly enhanced cGMP with no effect of NO. BI 685509 increased cGMP in human and rat platelet-rich plasma treated with the heme-oxidant ODQ; respective EC_{50} values were 467 nM and 304 nM. In conscious telemetry-instrumented rats, BI 685509 did not affect mean arterial pressure (MAP) or heart rate (HR) at 3 and 10 mg/kg (p.o.), whereas 30 mg/kg decreased MAP and increased HR. Ten days of BI 685509 at supratherapeutic doses (60 or 100 mg/kg p.o., daily) attenuated MAP and HR responses to a single 100 mg/kg challenge. In the ZSF1 rat model, BI 685509 (1, 3, 10, and 30 mg/kg per day, daily) coadministered with enalapril (3 mg/kg per day) dose-dependently reduced proteinuria and incidence of glomerular sclerosis; MAP was modestly reduced at the higher doses versus enalapril. In the 7-day rat unilateral ureteral obstruction model, BI 685509 dose-dependently reduced tubulointerstitial fibrosis ($P < 0.05$ at 30 mg/kg). In conclusion, BI 685509 is a potent, orally bioavailable sGC activator with clear renal protection and antifibrotic activity in preclinical models of kidney injury and disease.

SIGNIFICANCE STATEMENT

BI 685509 is a novel small soluble guanylate cyclase (sGC) molecule activator that exhibits an in vitro profile consistent with that of an sGC activator. BI 685509 reduced proteinuria and glomerulosclerosis in the ZSF1 rat, a model of diabetic kidney disease (DKD), and reduced tubulointerstitial fibrosis in a rat 7-day unilateral ureteral obstruction model. Thus, BI 685509 is a promising new therapeutic agent and is currently in phase II clinical trials for chronic kidney disease and DKD.

Introduction

Soluble guanylate cyclase (sGC) serves as a receptor for nitric oxide (NO) and is the key signal-transduction enzyme in the NO-cyclic guanosine monophosphate (cGMP) pathway. Diminished responsivity of the NO-cGMP pathway has been implicated in the pathogenesis of cardiovascular and kidney diseases, conditions associated with elevated oxidative stress. Thus, drug discovery research efforts have centered on improvement of sGC function using small molecule modulators for the treatment of human diseases, including chronic kidney disease (CKD).

sGC is a heterodimeric protein complex comprised of α- and β-subunits with a heme prosthetic group located in the β-subunit. NO, a transient and locally acting signaling molecule, exerts its action by binding to the heme prosthetic group to induce a conformational change that stabilizes the protein in a catalytically active state, thus enabling conversion of GTP to cGMP. cGMP modulates the activity of multiple downstream targets, including

This work received no external funding.
All authors were employed at Boehringer Ingelheim Pharmaceuticals at the time the research was performed.
No author has an actual or perceived conflict of interest with the contents of this article.
dx.doi.org/10.1124/jpet.122.001423.
[S] This article has supplemental material available at jpet.aspetjournals.org.

ABBREVIATIONS: α-SMA, α smooth muscle actin; ACEi, angiotensin-converting enzyme inhibitor; ARB, angiotensin receptor blocker; AUC, area under the curve; cGMP, cyclic guanosine monophosphate; CKD, chronic kidney disease; DKD, diabetic kidney disease; ESRD, end-stage renal disease; HR, heart rate; KIM-1, kidney injury molecule 1; MAP, mean arterial pressure; NGS, next-generation sequencing; NO, nitric oxide; PRP, platelet-rich plasma; sGC, soluble guanylate cyclase; TIF, tubulointerstitial fibrosis; UPE, urinary protein excretion; UUO, unilateral ureteral obstruction.

protein kinase G, cyclic nucleotide-gated ion channels, and phosphodiesterases (Stasch et al., 2001).

Conditions of persistent oxidative stress occur in patients with diabetes, cardiovascular diseases, and chronic/diabetic kidney disease and are associated with increased levels of reactive oxygen species. Reactive oxygen species can oxidize the heme iron of sGC, converting Fe^{2+} to Fe^{3+}, which destabilizes the heme group and can lead to its loss, and react directly with NO, thereby decreasing its abundance. Thus, elevated oxidative stress induces deficiencies of NO and cGMP signaling through a variety of mechanisms (Gillis et al., 2018).

Two classes of compounds, termed stimulators and activators, have been identified, which restore cGMP production by sGC through differing mechanisms. The sGC stimulators enhance cGMP generation in the absence and presence of NO when the iron within the heme prosthetic group is in a reduced state (Stasch et al., 2001). In contrast, sGC activators increase cGMP synthesis independently of NO through interactions in the heme binding site that stabilize the enzyme in a catalytically active conformation (Stasch et al., 2002). Oxidation or loss of the heme prosthetic group renders the enzyme nonfunctional and nonresponsive to sGC stimulators (Stasch et al., 2001), whereas sGC activators are optimally active under these conditions since binding requires displacement of the heme group (Stasch et al., 2006). These mechanisms are nicely depicted in a review by Stasch et al. (2015).

Diabetic kidney disease (DKD) is the leading cause of kidney failure or end-stage renal disease (ESRD) in the developed world (Koye et al., 2018; Tuttle et al., 2014). Until recently, approved treatment options for DKD have been limited to the angiotensin converting enzyme inhibitors (ACEi) and angiotensin receptor blockers (ARB). Although ACEi/ARB were the standard of care for two decades, many treated patients continued to progress to ESRD (Lewis et al., 1993; Brenner et al., 2001; Lewis et al., 2001). Although the recent approval of SGLT2 inhibitors for treatment of CKD and/or DKD expand the previous limited standard of care, considerable unmet medical need persists, and additional therapies are required for disease management.

The progression of DKD has been linked to impaired endothelial function. Evidence to support the role of endothelial dysfunction in contributing to DKD is provided by polymorphisms in endothelial nitric oxide synthase, which lead to reduced enzyme activity, increased risk of disease (Dellamea et al., 2014), and an association of elevated plasma levels of endothelial dysfunction biomarkers with disease progression (Lajer et al., 2008; Persson et al., 2008; Hanai et al., 2009). A potential new approach to the treatment of DKD would be to directly augment sGC activity to restore signaling within this pathway and, in turn, bypass defects associated with reduced NO production by endothelial nitric oxide synthase.

Previously, we demonstrated that sGC activator monotherapy reduced renal injury in the ZSF1 model of DKD (Boustany-Kari et al., 2016). We hypothesized that sGC activator treatment would provide added therapeutic benefit in the ZSF1 model when coadministered with a clinically relevant dose of enalapril, an ACEi representing standard of care. The present report highlights the pharmacology of BI 685509, a novel, potent, and selective clinical-stage sGC activator, currently in phase II for CKD (NCT04736628) and DKD (NCT04750577). In addition to presenting the relevant in vitro pharmacology, we demonstrate the ability of BI 685509 to attenuate disease progression in the ZSF1 rat model when coadministered enalapril, thereby demonstrating the potential of BI 685509 to deliver therapeutic benefit to patients receiving standard therapy of ACEi/ARB. Finally, since tubulointerstitial fibrosis (TIF) is a known predictor of progression of CKD, we also demonstrate the antifibrotic effect of BI 685509 in the rat unilateral ureteral obstruction (UUO) model, a rapid preclinical model of tubulointerstitial fibrosis.

Materials and Methods

All in vivo studies were conducted in accordance with the Guide for the Care and Use of Laboratory Animals as adopted and promulgated by the US National Institutes of Health and under an Institutional Animal Care and Use Committee-approved study protocol at Boehringer Ingelheim Pharmaceuticals, Inc., Ridgefield, CT 06877, or in accordance with the German and European Animal Welfare Act and authorized by the Regierungspräsidium Tübingen as the responsible local German authority.

The methods used to perform the primary pharmacology studies are detailed below, whereas methods for supporting assays and models are detailed in the Supplemental Information Materials and Methods document available online. The supplemental information includes a detailed description of materials and methods relevant to rat cardiovascular (telemetry) studies; pharmacokinetic studies, including pharmacokinetic/pharmacodynamic modeling; tissue collection and processing, including assessment of renal histopathology; and next-generation sequencing.

sGC Activity Assay

Recombinant reduced and heme-free human sGC were generated as previously described (Nedvetsky et al., 2002). Enzyme (0.2 nM reduced or 0.1 nM heme free), 1 mM DETA NONate (when included), and compounds were preincubated at room temperature for 10 minutes in reaction buffer (50 mM MOPS, pH 6.8; 5 mM $MgCl_2$; 50 mM NaCl; 0.2 mM TCEP; 1 mM IBMX; 0.1% bovine serum albumin). GTP at a final concentration of 50 μM was added to initiate the reaction for 30 minutes at 37°C. Cyclic GMP was quantified in a competitive immunoassay using homogenous time-resolved fluorescence following the manufacturer instructions (Cisbio, Bedford, MA).

Human Platelet-Rich Plasma Assay

Human forearm blood was drawn aseptically under informed consent by veni-puncture using a 21-gauge needle from healthy human volunteers. Blood was collected into Vacutainer glass tubes containing 3.2% sodium citrate, poured into 50 mL conical centrifuge tubes, and centrifuged for 16 minutes at 200*g* at room temperature. The upper platelet-rich plasma layer was collected, and 35 μL was transferred to a 96-well half-area plate and incubated at 37°C for 10 minutes. Thirty-five microliters of BI 685509 was added and incubated at 37°C for 10 minutes. In a 384-well Low Volume Black Round Bottom Polystyrene NBS Microplate, 10 μL platelet-rich plasma (PRP) incubation reaction solution, 5 μL of cGMP-XL665 conjugate, and 5 μL anti-cGMP cryptate conjugate were combined and incubated at room temperature for 60 minutes in the dark. Cyclic GMP concentration was quantified in a competitive immunoassay using homogenous time-resolved fluorescence.

ZSF1 Model of Diabetic Kidney Disease

Animals. Sixty male ZSF1 obese rats were obtained from Charles River Laboratories (Kingston, NY) following surgical implantation of telemetry transmitters (Data Sciences International, Inc., PA11TA-C40) in the abdominal artery to allow for continuous monitoring of mean arterial pressure (MAP) and heart rate (HR). Rats were

acclimated to metabolism cages (Laboratory Products, Inc., Seaford, DE) for 11 days prior to baseline collections and remained in these cages throughout the study to allow for weekly collection of urine. Two baseline urine measurements were collected. The first baseline (pretest) was collected over 8 days (14 to 15 weeks of age), and the rats were subsequently separated into two groups based on urinary protein excretion (UPE), MAP, HR, and body weight. Animals assigned to treatment (n = 50 in total) received enalapril (3 mg/kg per day in 1% Pluronic F127/DI water, 5 mL/kg p.o.) lead-in prior to randomization into treatment groups, whereas the untreated animals (n = 10) received vehicle alone (1% Pluronic F127/DI water). Thereafter, a second baseline used to assign animals to the study groups was collected during the enalapril lead-in phase of the study (9 days). The animals assigned to treatment (16 to 17 weeks of age) were next assigned into specific groups based on their average second baseline UPE, MAP, HR, and body weight; treatment groups received either enalapril (3 mg/kg per day, p.o., n = 10) or one of four doses of BI 685509 (1, 3, 10, or 30 mg/kg per day) in combination with enalapril (3 mg/kg per day, p.o.; n = 10/group).

A general study protocol for ZSF1 (and UUO) studies is shown in Supplemental Fig. 1. All oral dosing was performed at a volume of 5 mL/kg. Throughout the study, rats had ad libitum access to diet (Purina Formulab 5008, WF Fisher & Son, Inc., Somerville, NJ). Rats were subsequently monitored for 10 weeks, during which body weight was recorded once per week and food intake and water intake thrice weekly. Urine was collected chilled once weekly over a 24-hour period for measurement of protein contents. Blood samples were collected at baseline, following 1, 4, and 7 weeks of treatment, and at study termination (week 10) for pharmacokinetic, clinical chemistry, plasma glucose, and HbA1c measurements. Hemodynamic parameters were recorded intermittently (30 seconds of continuous data every 10 minutes), and weekly 24-hour averages were calculated. At study end, rats were sacrificed under isoflurane anesthesia by exsanguination through cardiac puncture, and kidneys were collected for histologic analysis.

UUO Model

Forty-eight 8-week-old male Sprague-Dawley rats from Taconic Bioscience were randomized into four groups: a sham group of eight rats with sham UUO surgery and 10 rats of each group for the remaining three UUO groups. UUO surgery is similar as described (Nagle et al., 1973) under isoflurane-induced anesthesia using aseptic techniques. A midline abdominal incision was made to access the kidney, and the left ureter was occluded and ligated at the level of the lower renal pole to induce irreversible UUO. The incision was closed, and the animals were allowed to recover under observation. During the study, all animals were orally dosed with either vehicle (1% Pluronic F127/DI water, 5 mL/kg) or test article BI 685509 at 10 or 30 mg/kg per day. Seven days postsurgery, animals were sacrificed, and the left kidney was collected for assessment of TIF and next-generation sequencing (NGS) data generation. Obstructed kidneys were sectioned transversally to generate a 3–5-mm slice in thickness, placed into a histocassette, and stored in 10% formalin for a minimum of 24 hours. After standard histologic processing, 4-μm thick paraffin-embedded tissue sections were placed on glass slides for Sirius Red morphometry staining and fibrosis analysis. For NGS analysis sample generation, 5–10 mg of cortical tissue from the obstructed kidney was collected and placed in RNALater overnight, then stored at −80°C prior to RNA extraction, quality control, and NGS data generation. Experimental animals had free access to food and water during the study.

Statistical Analysis

Data collected repetitively over time were analyzed using a two-way ANOVA with repeated measures and a Bonferroni post hoc analysis. Data obtained through single measurements (histologic endpoints) were analyzed using a one-way ANOVA with Tukey's post hoc analysis. Data were plotted as mean ± S.E.M., with a P value ≤ 0.05 considered statistically significant. Statistical analysis was performed using GraphPad Prism Version 6.01 (GraphPad Software, Inc., La Jolla, CA).

Results

In Vitro Profile of a Novel sGC Activator. sGC enzyme exists in different biologically relevant forms, each characterized by the status of the iron heme prosthetic group: the native form of sGC functions as the biological "receptor" for NO and is the heme-containing, reduced form. Additional forms of sGC are the oxidized and heme free that no longer bind NO and are catalytically inactive. Meanwhile, sGC activators and stimulators are differentiated by the specific cGMP response profile each generates. sGC stimulators are heme dependent with regard to inducing cGMP generation, whereas sGC activators are heme independent; also, sGC activators can potently augment cGMP production in the absence of NO, especially when the sGC enzyme is heme free (Stasch et al., 2006). Using human sGC $\alpha1\beta1$ heterodimer containing a reduced heme group, BI 685509 (Fig. 1) produced concentration-dependent increases in cGMP that were elevated modestly in the presence of NO (Fig. 2A). Moreover, heme-free sGC tested with increasing concentrations of BI 685509 displayed greatly enhanced cGMP generation, an effect that was not altered by the presence of NO, consistent with the profile of an sGC activator (Fig. 2A).

In contrast, praliciguat, an sGC stimulator (Tobin et al., 2018), had no effect on heme-free sGC activity in the presence or absence of NO. However, under conditions of a reduced sGC

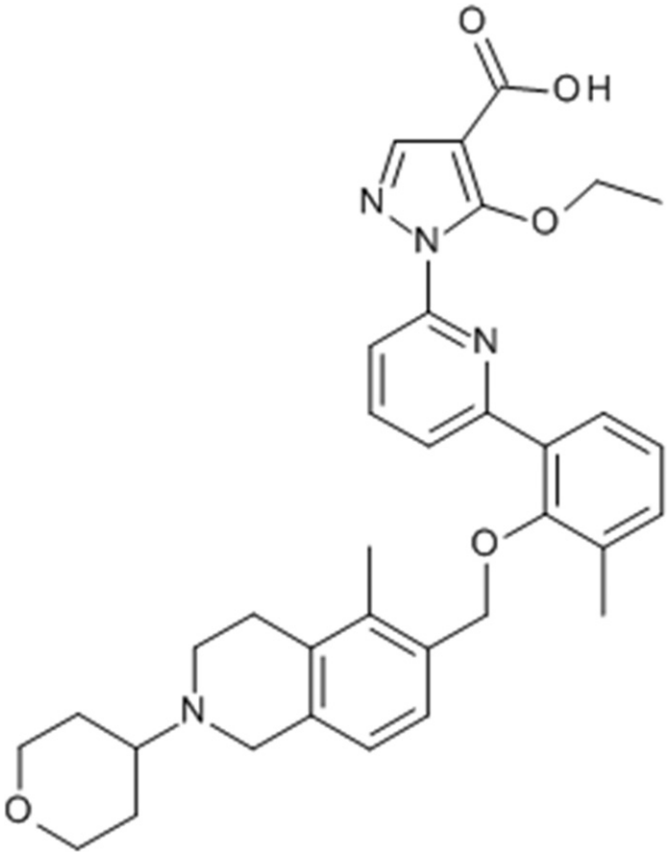

Fig. 1. Structure of BI 685509.

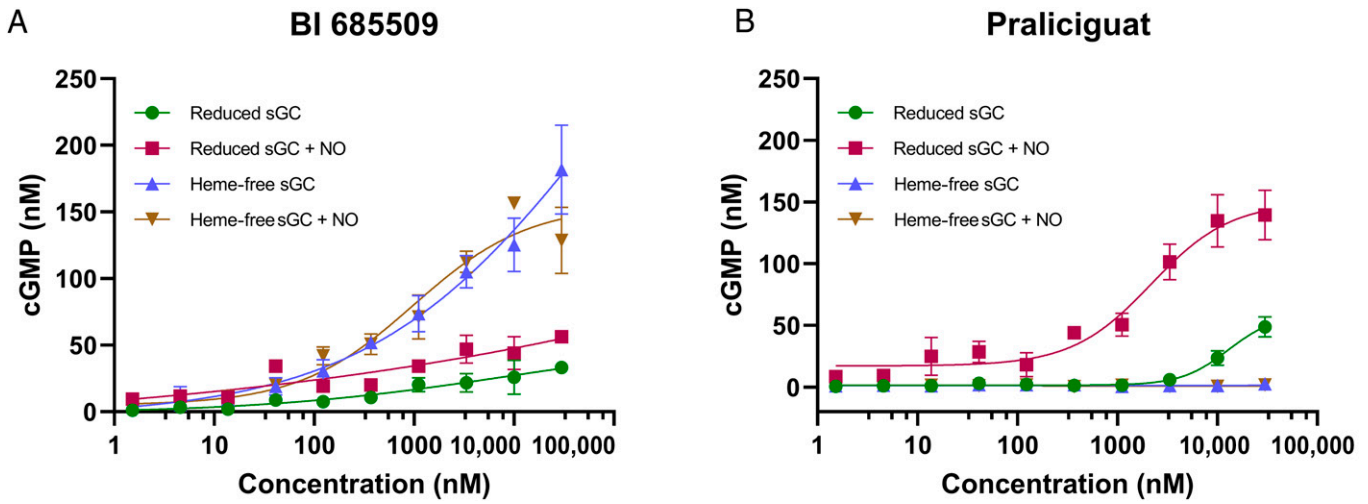

Fig. 2. (A) Concentration-dependent effect of sGC activator BI 685509 and (B) the sGC stimulator praliciguat on cGMP generation from human sGC $\alpha1\beta1$ heterodimer containing a reduced heme group (Reduced sGC) or no heme group (Heme-free sGC) in the presence and absence of NO.

heme group, praliciguat produced a concentration-dependent increase in cGMP, a response that was greatly shifted leftward and upward by NO (Fig. 2B) and is consistent with that of an sGC stimulator.

In further experiments, the ability of recombinant sGC $\alpha1/\beta1$, heme-free enzyme to be activated by BI 685509 was tested for different animal species and using the human $\alpha2/\beta1$ enzyme. BI 685509 increased cGMP production with an EC_{50} of 9.29, 3.52, 4.69, 8.65, and 5.54 nM against the mouse, rat, dog, cynomolgus monkey, and human $\alpha2/\beta1$ enzyme, respectively, compared with an EC_{50} of 6.81 nM against the human $\alpha1/\beta1$ enzyme.

BI 685509 increased cGMP levels in human PRP treated with the heme-oxidant 1H-[1,2,4] Oxadiazolo[4,3-a]quinoxalin-1-one (ODQ) with an EC_{50} of 467 nM (Fig. 3). In rat PRP in which sGC was similarly oxidized, BI 685509 increased cGMP with an EC_{50} of 304 nM, demonstrating good congruency across species in a more complex system expected to better mimic the in vivo condition by accounting for plasma protein binding.

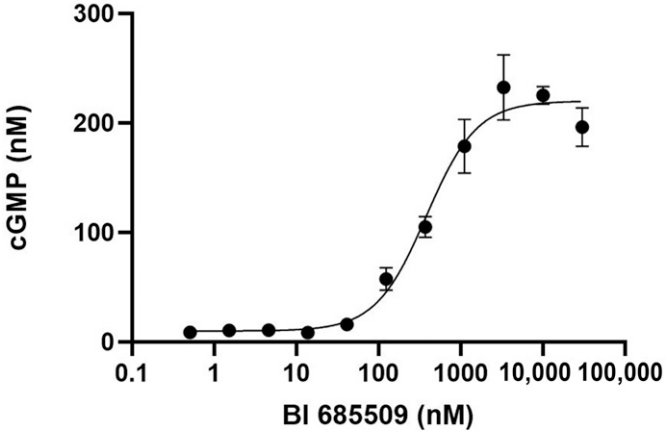

Fig. 3. Concentration-dependent effect of BI 685509 on cGMP levels in human PRP from four volunteers treated with the heme-oxidant ODQ, yielding an average EC_{50} of 467 nM.

Pharmacokinetic Profile—Mouse and Rat PK Properties. Following oral gavage dosing in mice or rats, BI 685509 was rapidly absorbed, achieving maximal plasma concentration at the first collection timepoint of 0.25 hours in both species (Supplemental Tables 1 and 2). After intravenous administration in rats, BI 685509 displayed a low volume of distribution at steady state of 1.05 L/kg and moderate clearance (32.1 mL/min per kg), leading to short half-life (~1.8 hour) and a moderate bioavailability of ~60%.

Telemetry Rat Blood Pressure and Heart Rate Profile—Single-Dose Study. During the 24-hour baseline period (values calculated every 10 minutes), MAP and HR values were similar across groups. BI 685509 at 3 or 10 mg/kg elicited no consistent reductions in MAP and no significant increase in HR compared with vehicle controls, although HR trended upward in response to treatment. In the 30-mg/kg dose group (and within 40 minutes postdose), MAP decreased significantly to 12–25 mmHg below baseline, whereas HR increased to 17% above baseline (Fig. 4, A and B). Although blood samples were not collected during the initial 8-hour observation period to avoid artifactual changes in MAP and HR, exposures from satellite animals (n = 4 to 5/group) exhibited C_{max} values of 60, 410, and 830 nM, respectively, for the doses used. These data suggest that a C_{max} as high as 410 nM BI 685509 exerted no significant, acute effects on blood pressure or HR. In addition, respective drug concentrations in telemetry animals at 8 hours postdose were 24 ± 5.9 nM, 41 ± 5.8 nM, and 201 ± 37.2 nM, concentrations consistent with the C_{max} values observed in the satellite animals.

Telemetry Rat Blood Pressure and Heart Rate Profile—10-Day Repeat-Dose Study. On day 1, BI 685509 at 60 or 100 mg/kg, per os, produced the expected dose-dependent decreases in MAP and corresponding elevations in HR, responses that were generally attenuated during the subsequent 10 days of successive dosing (Fig. 4C). On the last day of the study (day 11), animals were challenged with a hypotensive dose of BI 685509 (100 mg/kg) to assess attenuation of the blood pressure response after repeated dosing. Reductions in MAP elicited by the 100 mg/kg challenge dose were not different in the vehicle animals compared with day 1 (t test). In contrast,

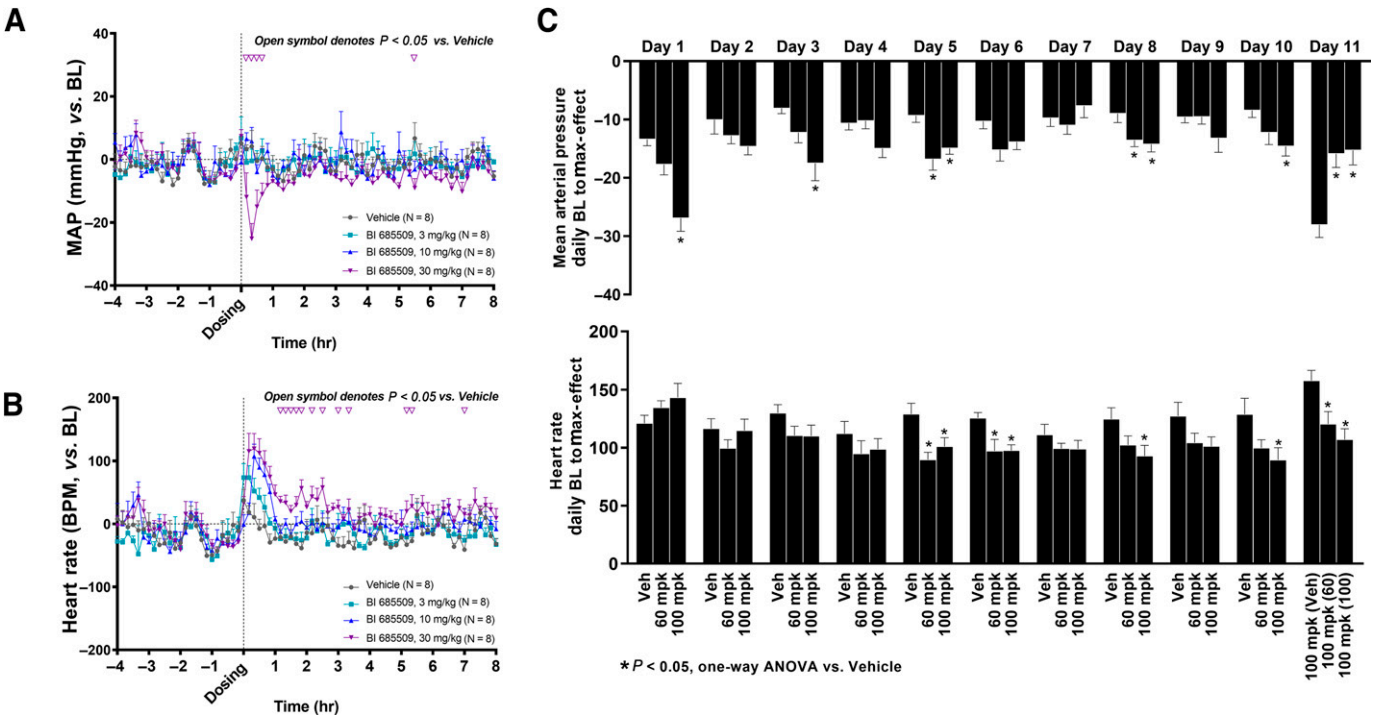

Fig. 4. Effect of sGC activation by BI 685509 on conscious (A) MAP and (B) HR after a single oral dose in telemetry-instrumented rats following a 24-hour baseline period. Open downward triangles denote $P < 0.05$ versus vehicle. (C) Daily effect of oral administration BI 685509 at supratherapeutic doses ($n = 12$/group) on conscious MAP and HR during a 10-day repeated treatment followed by a single oral challenge of BI 685509 at 100 mg/kg on the final day to assess attenuation of responses. Mean values for each group were compared each day by one-way ANOVA with Dunnett's post-test versus vehicle without adjusting for repeated measures ($P < 0.05$), as indicated by asterisk.

acute reductions in MAP produced by the 100-mg/kg challenge of BI 685509 were significantly attenuated following 10 days of repeat dosing in the 60- and 100-mg/kg treatment groups. Similarly, acute increases in HR produced by the 100-mg/kg BI 685509 challenge were significantly attenuated following repeat dosing of BI 685509 compared with vehicle (Fig. 4C). Collectively, these data demonstrate that the initial, acute depressor and HR responses to high doses of BI 685509 attenuate markedly in response to repeated dosing, an effect that becomes apparent as early as the second day of treatment.

Effect of BI 685509 in the Rat ZSF1 Model of Diabetic Kidney Disease. Mean plasma concentrations of BI 685509 across weeks 1, 4, 7, and 10 in animals treated with 1, 3, 10, or 30 mg/kg per day, per os, in combination with enalapril (3 mg/kg per day) are shown in Supplemental Fig. 2. At 1 hour postdose, mean plasma concentrations of BI 685509 were 226 ± 122, 485 ± 161, 2210 ± 616, and 1610 ± 340 nM. Exposure for the 10- and 30-mg/kg-per-day doses were roughly similar across the measured time points of 1, 6, and 24 hours (although the 24-hour values showed dose dependence), suggesting that rate-limited absorption may be occurring at doses >10 mg/kg per day. Meanwhile, plasma concentrations of enalaprilat, the active metabolite of enalapril, were comparable across the different treatment groups (Supplemental Fig. 2).

Body weight and food and water intake were not significantly different between study groups (Supplemental Fig. 3) at baseline or during BI 685509 treatment plus enalapril or enalapril alone throughout the 10-week observation period.

HbA1c levels and nonfasting plasma glucose following BI 685509 plus enalapril were not significantly different from either vehicle or enalapril (change from baseline HbA1c%: 1.0 ± 0.3, 1.2 ± 0.5, 1.4 ± 0.5, 1.4 ± 0.4, 1.1 ± 0.5, and 0.7 ± 0.7; change from baseline plasma glucose: 10.4 ± 24.1, 116.1 ± 20.8, 75.6 ± 34.9, 122.9 ± 23.3, 101.2 ± 37.5, and 140.8 ± 33.5 mg/dL for vehicle, enalapril, and BI 685509 at 1, 3, 10, and 30 mg/kg per day, respectively, in combination with enalapril; $P > 0.05$).

At baseline (following enalapril lead-in dosing), there was no significant difference in MAP or HR between the BI 685509 plus enalapril combinations and enalapril alone study groups (MAP: 114 ± 2, 108 ± 1, 106 ± 1, 111 ± 2, 110 ± 2, and 106 ± 2 mmHg; HR: 284 ± 4, 283 ± 4, 279 ± 2, 294 ± 4, 290 ± 5, and 285 ± 2 beats per minute for vehicle, enalapril, and BI 685509 at 1, 3, 10, and 30 mg/kg per day, respectively, in combination with enalapril; $P > 0.05$). BI 685509 at 30 mg/kg per day plus enalapril (3 mg/kg per day) significantly reduced MAP compared with both vehicle and enalapril alone from study week 1 onward (Fig. 5A). Lower doses of BI 685509 plus enalapril significantly reduced MAP at 10, 3, and 1 mg/kg per day beginning on weeks 2, 3, and 4, respectively, versus vehicle and beginning on week 2 at 10 mg/kg per day compared with enalapril alone. In comparison, enalapril alone only significantly reduced MAP versus vehicle from week 7 onward.

HR decreased steadily over time in all study groups, including vehicle (Fig. 5B), and the magnitude of decline was less pronounced as the dose of BI 685509 increased and MAP reductions were more prominent. BI 685509 at 30 and 10 mg/kg per day plus enalapril significantly increased HR beginning on weeks 1 and 9, respectively, compared with enalapril alone, whereas BI 685509 30 mg/kg per day plus enalapril exhibited significant increases in HR on weeks 1, 2, 3, and 8 compared with vehicle. There was no significant effect of BI 685509 at

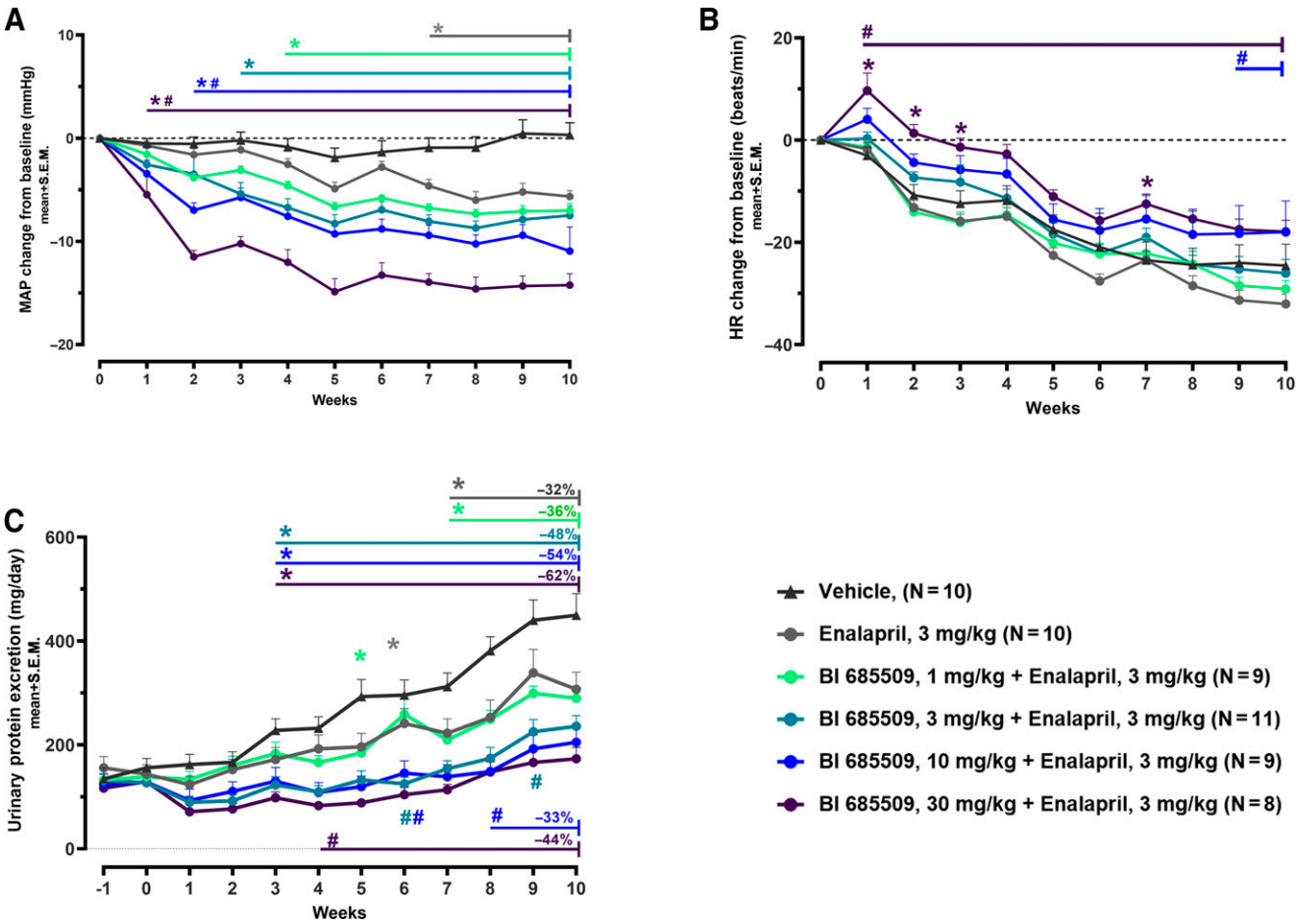

Fig. 5. Effect of sGC activation on MAP, HR, and UPE. (A) Weekly MAP in ZSF1 rats. Lower doses of BI 685509, in combination with enalapril, showed significant reductions in MAP at 30, 10, 3, and 1 mg/kg beginning on weeks 2, 3, and 4, respectively, compared with vehicle and beginning on week 2 at 10 mg/kg compared with enalapril alone. Enalapril at 3 mg/kg elicited significant reductions in MAP at weeks 7–10 compared with vehicle. (B) Weekly HR in ZSF1. BI 685509 at 30 and 10 mg/kg, in combination with enalapril (3 mg/kg), resulted in significantly higher HR beginning on weeks 1 and 9 compared with enalapril alone. (C) Weekly UPE in ZSF1 rats. BI 685509 at 30 and 10 mg/kg, in combination with enalapril (3 mg/kg,) significantly reduced UPE levels from weeks 4 and 8 onwards, respectively, versus enalapril alone. BI 685509, in combination with enalapril, showed significant reductions in UPE at 30, 10, 3, and 1 mg/kg beginning on weeks 3, 3, 3, and 7 compared with vehicle. * and # signify statistical significance compared with vehicle and enalapril, respectively ($P < 0.05$, two-way ANOVA with repeated measures and Bonferroni post hoc analysis).

1, 3, or 10 mg/kg per day in combination with enalapril or enalapril alone on HR compared with vehicle.

There was no significant difference in UPE at baseline between study groups (UPE: 156 ± 18, 144 ± 18, 141 ± 10, 127 ± 14, 125 ± 20, and 130 ± 10 mg/d for vehicle, enalapril, and BI 685509 at 1, 3, 10, and 30 mg/kg per day in combination with enalapril, respectively; $P > 0.05$). Administration of BI 685509 at 30 and 10 mg/kg per day plus enalapril significantly reduced UPE levels from weeks 4 and 8 onward, respectively, compared with enalapril alone (Fig. 5C). BI 685509 plus enalapril showed significant reductions in UPE at 30, 10, 3, and 1 mg/kg per day beginning on weeks 3, 3, 3, and 7, respectively, compared with vehicle. Enalapril (3 mg/kg per day) significantly reduced UPE levels versus vehicle from week 7 onwards.

To determine BI 685509 in vivo potency in reducing UPE, individual mean plasma concentrations were correlated with an overall UPE change from baseline [area under the curve (AUC)] utilizing an inhibitory effect I_{max} model (Fig. 6, A and B). An IC_{50} of 213 nM C_{max} (63.4% CV) and 1210 nM*hr (63.5% CV) AUC was predicted to reduce UPE by 50% on top of enalapril, a value that is close to that of the rat PRP EC_{50} (304 nM).

Kidney-weight to body-weight ratios for left and right kidneys were not different after 10 weeks of BI 685509 plus enalapril or enalapril alone. The average left kidney weight/body weight ratios were: vehicle, 0.415 ± 0.015; enalapril, 0.413 ± 0.034; BI 685509 in combination with enalapril, 0.402 ± 0.012, 0.392 ± 0.017, 0.376 ± 0.018, and 0.382 ± 0.017 at 1, 3, 10, and 30 mg/kg per day, respectively. The average right kidney weight/body weight ratios were: vehicle, 0.416 ± 0.021; enalapril, 0.405 ± 0.016; BI 685509 in combination with enalapril, 0.389 ± 0.009, 0.381 ± 0.014, 0.380 ± 0.016, and 0.382 ± 0.017 at 1, 3, 10, and 30 mg/kg per day, respectively.

Incidence of glomerulosclerosis was slightly reduced by enalapril (3 mg/kg per day; 7.4% ± 1.8% decrease versus vehicle; $P > 0.05$) without achieving statistical significance. In contrast, BI 685509 plus enalapril dose-dependently reduced the incidence of glomerulosclerosis, with reductions achieving statistical significance in both the 10- and 30-mg/kg-per-day groups compared with both enalapril alone and vehicle (Figs. 7

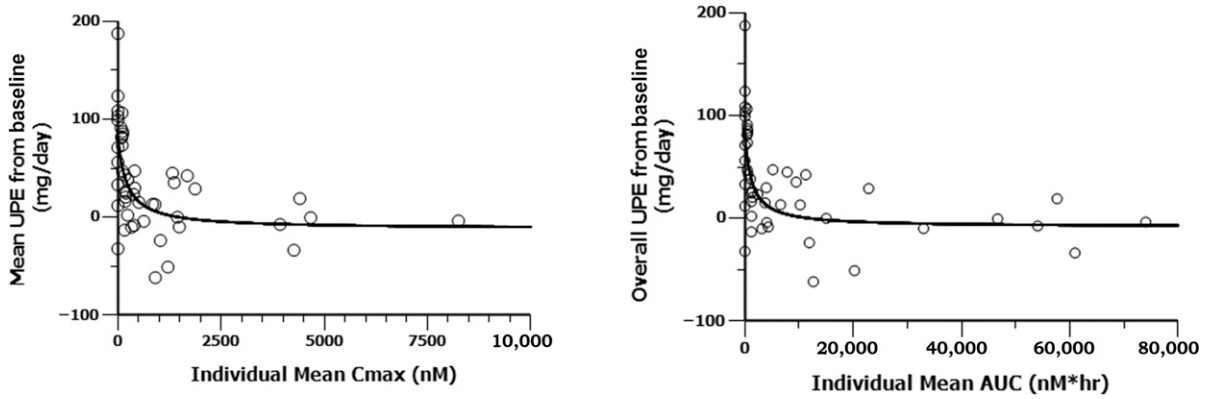

Fig. 6. Correlation of BI 685509 plasma exposure with UPE. (A) Individual mean C_{max} (nM) versus mean UPE and (B) individual mean AUC (nM*hr) versus mean UPE. Using a simple inhibitory effect I_{max} model, BI 685509 individual mean plasma concentrations from weeks 1, 4, 7, and 10 were correlated with the mean UPE levels (mg/d) from baseline for individual animals. Decreasing UPE levels correlated with increasing BI 685509 plasma exposure. An IC_{50} of 213 nM C_{max} (63.4% CV) and 1210 nM*hr (63.5% CV) AUC was predicted to reduce UPE by 50% on top of enalapril.

and 8). Mean reductions in glomerular sclerosis incidence were similar for the 10- and 30-mg/kg BI 685509 plus enalapril groups.

A limitation of the rat ZSF1 model is the lack of development of TIF and other features of advanced kidney disease, including a reduction in glomerular filtration rate. To ascertain whether BI 685509 treatment modulated early markers of disease mechanisms including fibrosis, tubular injury, and inflammation, α smooth muscle actin (α-SMA), kidney injury molecule 1 (KIM-1), and ED-1, respectively, were quantified in kidney cortex tissue by immunohistochemistry. BI 685509 plus enalapril significantly reduced α-SMA expression at all doses tested compared with vehicle and at doses of 3, 10, and 30 mg/kg per day compared with enalapril alone (Table 1). Enalapril (3 mg/kg per day) modestly and significantly reduced α-SMA expression. BI 685509 plus enalapril significantly reduced KIM-1 expression at 3 and 10 mg/kg per day compared with vehicle (Table 1). Enalapril alone did not result in a significant reduction in KIM-1 expression ($P > 0.05$). Numerical reductions in ED-1 expression not achieving statistical significance were observed in BI 685509 plus enalapril and enalapril alone groups (Table 1). In addition, urinary KIM1 and NGAL were not statistically different compared with enalapril across the BI 685509 treatment groups.

Effect of BI 685509 in the Rat UUO Model of Tubulointerstitial Fibrosis. With TIF reported as percentage of fibrotic (Sirius Red stained) area, 7 days of UUO induced a ~3.5-fold fibrosis increase in vehicle UUO group compared with sham (**$P < 0.01$, Fig. 9). BI 685509 dose-dependently decreased TIF in comparison with vehicle; the 10-mg/kg dose reduced TIF to 10.7% ± 0.7% below sham, a response that did not achieve statistical significance, whereas the 30-mg/kg dose significantly reduced TIF to values 17.9% ± 0.8% below sham (*$P < 0.05$) versus vehicle.

In NGS analysis of tissue from UUO kidneys, principal component analysis showed the samples to be well grouped by experimental condition, with the sham surgery segregating from the UUO treatment in principal component 1 and the BI 685509–treated animals separating from vehicle treatment in principal component 2 (Fig. 10A). The two dose groups did not separate within the principal components and, additionally, had a high degree of concordance in their differentially expressed genes when compared with the vehicle-treated group, indicating qualitatively similar pharmacodynamic effects (Supplemental Fig. 4). These two doses were combined for later analyses. The differential gene expression analysis on the RNA samples from the UUO model yielded 231 genes when comparing the vehicle and combined BI 685509–treated groups (Fig. 10B; Supplemental Table 3). This signature included downregulation of four genes associated with urea transport (Slc14a1, Slc14a2, Upk3a, and Aqp3) with BI 685509 treatment (Supplemental Fig. 5). Additional analysis showed downregulation by BI 685509 of many key genes associated with the development of extracellular matrix, which had increased in the vehicle group, consistent with the observed effect on histology (Supplemental Fig. 6). Key podocyte markers, including Nphs1, Nphs2, and Podxl, showed reduced expression to a lesser degree in the BI 685509–treated animals compared with the vehicle group (Supplemental Fig. 7).

Discussion

We describe a novel, clinical-stage sGC activator, BI 685509, which demonstrates renoprotective effects in two models of kidney disease. Our in vitro studies defined BI 685509 as a potent activator of heme-free human sGC enzyme, producing concentration-dependent increases in cGMP that were independent of NO. BI 685509 demonstrates low-nM potency for sGC $\alpha1\beta1$ activation across multiple mammalian species and the human $\alpha2/\beta1$ enzyme. As expected, the in vitro profile of BI 685509 contrasts with that of an sGC stimulator such as praliciguat (Tobin et al., 2018), which displayed a clear lack of activity in the absence of heme.

In human PRP, a more complex in vitro model with greater in vivo relevance compared with the molecular assays due to plasma protein binding, BI 685509 increased cGMP in a concentration-dependent fashion. BI 685509 increased cGMP in human and rat PRP with an EC_{50} of 370 nM and 304 nM, respectively. In the ZSF1 rat, coadministration with enalapril producing BI 685509 exposures that exceeded the PRP EC_{50} by ~three- to fourfold delivered significant reductions in UPE and reduced the incidence of glomerular sclerosis when compared with the effects of enalapril alone. Moreover, when the ZSF1 UPE and individual mean plasma concentrations of BI 685509 from weeks 1, 4, 7, and 10 were correlated in an inhibitory effect I_{max} model, an IC_{50} of 213 nM was observed, a concentration similar to the rat PRP EC_{50} of 304 nM. These data, in

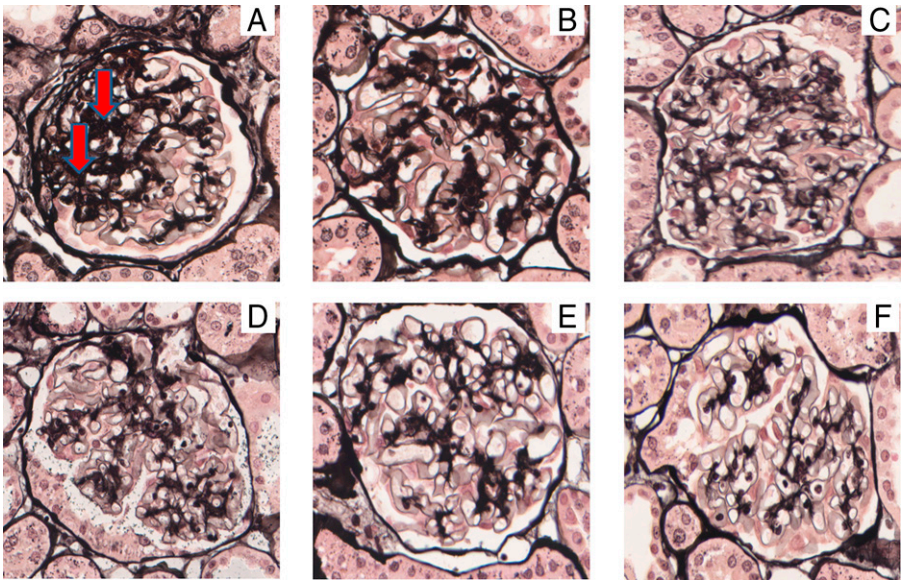

Fig. 7. Effect of sGC activation in combination with enalapril on glomerular lesions. Representative glomerulosclerosis from (A) vehicle, (B) enalapril at 3 mg/kg, and (C–F) BI 685509 at 1, 3, 10, and 30 mg/kg in combination with enalapril at 3 mg/kg, respectively. Red arrows indicate areas of advanced glomerular sclerosis in the vehicle control tissue. Based on semi-quantative glomerular scoring of 25 random glomeruli (1+, showing segmental condensation and structural collapse of approximately one quarter of the glomerular area; 2+, showing segmental condensation and structural collapse of half of the glomerular area; and 3+ showing condensation and structural collapse of most of the glomerular area), BI 685509 dose-dependently reduced glomerulosclerosis compared with enalapril alone.

addition to demonstrating pharmacologic congruency between the PRP assay and the ZSF1 disease model, suggest the potential for BI 685509 to exert disease-modifying effects in patients with persistent oxidative stress, such as CKD/DKD patients, at nanomolar exposures, a hypothesis to be tested in current clinical trials.

In addition to being a selective and potent sGC activator, BI 685509 is orally bioavailable with rapid absorption in mouse and rat and, at a dose of 30 mg/kg, elicits transient reductions in blood pressure and concomitant elevations in heart rate in the conscious rats. These acute blood pressure reductions were associated with a C_{max} of 830 nM, a value well above the rat PRP of 304 nM, whereas a C_{max} of 410 nM had no effect. Given that acute reductions in blood pressure are not desirable at clinically relevant doses, we assessed whether repeated administration of supratherapeutic, depressor doses of BI 685509 would moderate any blood pressure changes. Our results demonstrate a clear attenuation of acute hemodynamic responses in the normal Sprague-Dawley rat following 10-day, repeat oral administration of supratherapeutic doses of BI 685509, a response that could not be assessed definitively in the ZSF1 study. In total, these results suggest that acute blood pressure responses are unlikely to increase over time and, importantly, that dose titration may be an effective means to minimize risk of blood pressure excursions in patients.

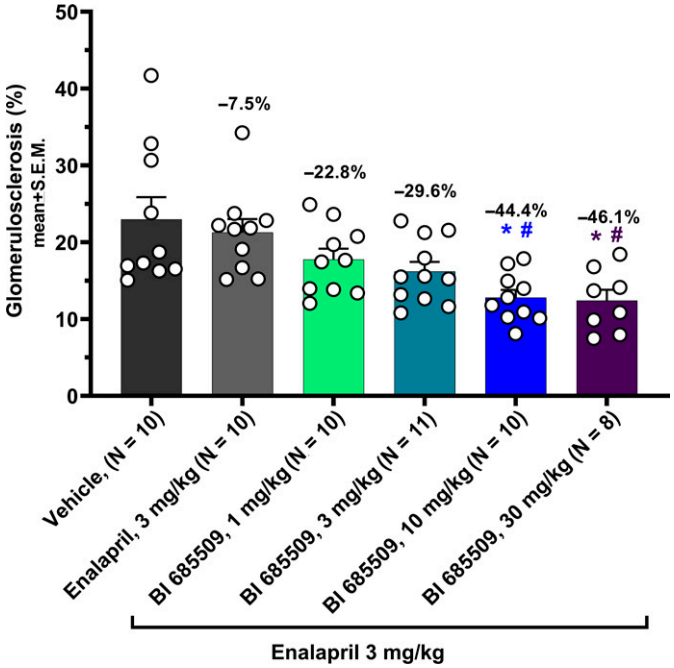

Fig. 8. Effect of sGC activation on incidence of glomerulosclerosis. BI 685509 in combination with enalapril (3 mg/kg) dose-dependently reduced the incidence of glomerulosclerosis (glomerulosclerosis %) and showed statistically significant reductions at 10 and 30 mg/kg compared with enalapril alone and vehicle. * and # signify statistical significance compared with vehicle and enalapril (3 mg/kg), respectively ($P < 0.05$, one-way ANOVA with Tukey's post hoc analysis).

We previously demonstrated that our earlier sGC activator BI 703704, when administered as a monotherapy, inhibited proteinuria and the incidence of glomerular sclerosis in the ZSF1 model of DKD and provided more robust renal protection compared with a clinically relevant dose of enalapril (Boustany-Kari et al., 2016). Here, we investigated the ability of BI 685509 to modulate disease progression in the ZSF1 rat when administered on top of the same dose of enalapril, reflecting the fact that ACEi/ARB have been the standard of care (and only approved drug classes) for the treatment of patients with DKD for nearly two decades. Oral administration of BI 685509 on top of an efficacious dose of enalapril was highly effective in preventing progression of DKD in the ZSF1 rat model at doses that produced little to modest reductions in MAP compared with enalapril alone. Treatment with BI 685509 plus enalapril for 10 weeks at 3, 10, and 30 mg/kg produced dose dependent, statistically significant decreases in UPE much earlier in the treatment period (week 3) than enalapril alone (week 3 versus week 7, respectively). Also, onset of reductions in UPE at week 1 preceded modest decrements in MAP in groups in which MAP was diminished, a response that typically did not reach steady state until week 5. These temporal differences suggest an early effect on glomerular

TABLE 1
Effect of sGC activation on tissue markers of renal damage
Tissue markers of renal damage, α-SMA, KIM-1, and ED-1, were quantified by immunohistochemistry and expressed as mean ± S.E.M. percent positive expression area/glomeruli and as a percent change from vehicle control.

Treatment	α-SMA		KIM-1		ED-1	
	% Positive Expression	Percent Change	% Positive Expression	Percent Change	% Positive Expression	Percent Change
Vehicle	6.40 ± 0.58		2.85 ± 0.43		1.89 ± 0.16	
Enalapril, 3 mg/kg	4.86 ± 0.45	−24.1[a]	2.42 ± 0.28	−15.4	1.79 ± 0.21	−5.3
BI 685509, 1 mg/kg + enalapril, 3 mg/kg	4.14 ± 0.35	−35.4[a]	2.94 ± 0.34	3.1	1.92 ± 0.19	2.0
BI 685509, 3 mg/kg + enalapril, 3 mg/kg	1.94 ± 0.17	−69.8[a,b]	1.54 ± 0.29	−45.9[a]	1.14 ± 0.25	−39.5
BI 685509, 10 mg/kg + enalapril, 3 mg/kg	2.54 ± 0.22	−60.4[a,b]	1.33 ± 0.17	−53.3[a]	1.24 ± 0.16	−34.3
BI 685509, 30 mg/kg + enalapril, 3 mg/kg	2.89 ± 0.39	−54.9[a,b]	1.58 ± 0.31	−44.6	1.09 ± 0.19	−42.3

[a]Significant $P < 0.05$ versus vehicle using one-way ANOVA.
[b]Significant $P < 0.05$ versus enalapril using one-way ANOVA.

filtration dynamics independent of subsequent reductions in systemic MAP. The relevance of these observations is twofold: they suggest a more rapid onset of reduced proteinuria compared with enalapril alone as well as an additive effect of BI 685509 when coadministered with an effective dose of enalapril. Finally, these data suggest that the sGC activator BI 685509 should not impede the renal benefits of ACEi/ARB therapy in DKD patients. These points are important as BI 685509 phase 2 clinical trials are being conducted in CKD and DKD patients on a stable dose of ACEi/ARB.

Glomerulosclerosis is a hallmark of DKD, and severity of glomerular lesions has been associated with disease progression and doubling of serum creatinine in type 2 diabetic patients with biopsy-proven DKD (An et al., 2015). Oral administration of BI 685509 plus enalapril produced dose-dependent decreases in the incidence of glomerular sclerosis in ZSF1 rats, whereas reductions induced by enalapril alone were not statistically significant. To our knowledge, this is the first report of an sGC activator coadministered with a clinically relevant dose of enalapril or equivalent antagonist of the renin-angiotensin system in a rodent model of DKD and also the first observation of reduced pathologic remodeling of glomerular structure under study conditions that more closely approximate a relevant clinical scenario. Viewed collectively, these observations suggest the potential for BI 685509 to demonstrate clinical efficacy on top of ACEis/ARBs, a long-standing standard of care for DKD and CKD patients.

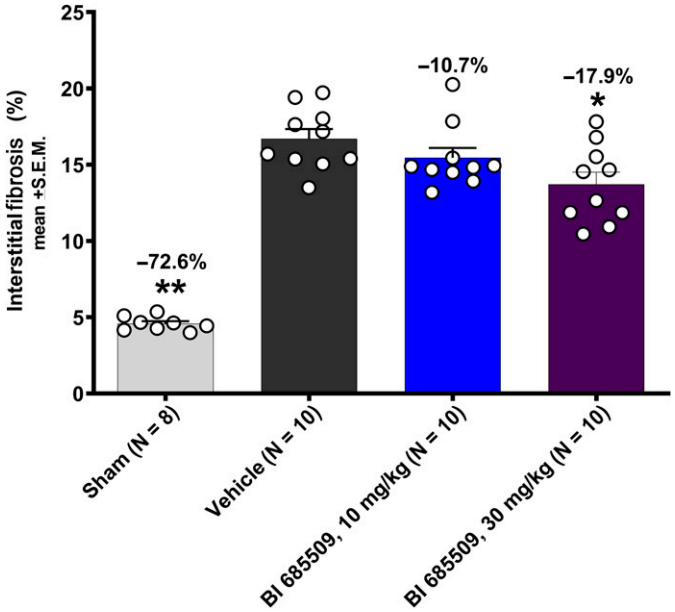

Fig. 9. Antifibrotic effect of sGC activation in 7-day rat UUO. BI 685509 reduced area of cortical tubulointerstitial fibrosis expressed as % of cortical area in sections stained with Sirius Red (**$P < 0.01$ versus vehicle; *$P < 0.05$ versus vehicle).

The properties of another advanced sGC activator, runcaciguat, have recently been described (Hahn et al., 2021), including demonstration of cardio- and renoprotective effects in several preclinical models of hypertensive and metabolic cardiorenal disease (Benardeau et al., 2021). Notably, chronic administration of runcaciguat to the Zucker diabetic fatty rat, a metabolic disease model displaying modest kidney pathology compared with the ZSF1 rat, attenuated proteinuria and biomarkers of kidney damage while inducing slight reductions in kidney damage parameters at doses associated with little to no effect on systolic blood pressure (tail cuff; Benardeau et al., 2021).

TIF has been increasingly recognized as another key hallmark of CKD and as the best predictor of kidney survival and ESRD (Nath, 1992; Gewin, 2018). TIF is a focal fibrotic renal event that is distinct from glomerulosclerosis and driven by sequalae downstream to tubular injury.

The ability of BI 685509 to reduce UUO-induced TIF in the present study is consistent with published studies of sGC stimulators in UUO and other models of kidney fibrosis (Stasch et al., 2015) and further demonstrates the potential clinical importance of sGC activators such as BI 685509 in the prevention of progression of DKD/CKD in humans. Consistent with reduced fibrogenesis, the expression of a subset of extracellular matrix genes was significantly induced in the UUO model and inhibited with BI 685509 treatment (Supplemental Fig. 6). This includes several collagens, such as Col1a1, which is reduced by treatment with BI 685509 and also has a strong correlation with morphometric measurements of TIF (Supplemental Fig. 8).

Another interesting observation from our NGS analysis of cortical samples from the UUO study is the reduced expression of urea-transport associate genes in response to BI 685509 treatment. The Slc14a2 gene (UT-A) encodes six isoforms of urea transporters. A recent study in UT-A1/A3 knockout mice reported a reduced renal fibrotic response to UUO, with a similar effect noted with urea transporter pharmacologic

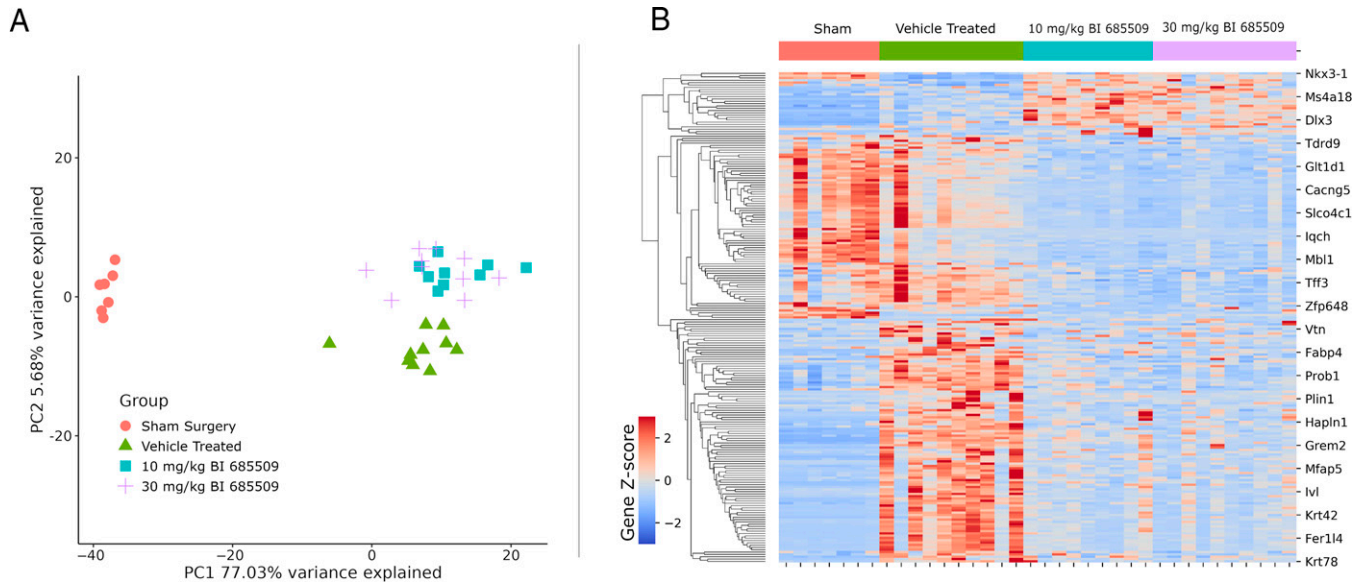

Fig. 10. UUO model RNA-sequencing (RNAseq) analysis. Principal component plot of samples from RNAseq experiment (A). Heatmap of gene expression values from genes selected for sGC-induced signature across doses, based on a false discovery rate threshold of <0.05 and a threshold of ± twofold change between groups (B).

inhibition (Rianto et al., 2020). Thus, it is plausible that the reduced expression of urea transporters (Slc14a1, Slc14a2, Upk3a, and Aqp3) with BI 685509 treatment could also contribute to the reduction in fibrosis observed in this study.

Additionally, although it is not anticipated that sGC activators would directly affect podocytes in the UUO model, we report evidence of reduced podocytopathy as a potential secondary effect since podocyte-associated genes, including Nphs1, Nphs2, and Podxl, for which expression is decreased in vehicle-treated UUO group, are partially preserved with BI 685509 treatment (Supplemental Fig. 7), concomitant with reductions in TIF. Given that recent studies have demonstrated that acute and repeated tubular-specific renal injury is able to elicit the full spectrum of renal fibrosis, including glomerulosclerosis (Grgic et al., 2012; Takaori et al., 2016), the concept of reduced podocytopathy in the UUO model in association with BI 685509–induced inhibition of TIF has merit and underscores the potential clinical benefit of the antifibrotic effects of sGC activators in patients with kidney disease.

In summary, BI 685509 is a potent and orally bioavailable sGC activator with clear disease-modifying potential. The ability of BI 685509 to reduce proteinuria and glomerular sclerosis dose dependently when coadministered on top of enalapril in a preclinical model of DKD, combined with a reduced TIF in the rat UUO model, gives credence to its therapeutic potential and provides strong rationale for continued phase II clinical development in patients with CKD/DKD.

Authorship Contributions

Participated in research design: Harrison, Sun, Wong, Fryer, Brenneman, Sarko, Boustany-Kari, Pullen.

Conducted experiments: Harrison, Lincoln, Chen, Sun, Clifford, Ng, Wang, Fowler, Gueneva-Boucheva, Zhang.

Contributed new reagents: Brenneman, Bosanac, Sarko.

Performed data analysis: Harrison, Lincoln, Sun, Hill, Qian, McHugh, Wang, Fowler, Gueneva-Boucheva, Wong, Fryer.

Wrote or contributed to writing of the manuscript: Reinhart, Harrison, Hill, Ng, Wong, Fryer, Boustany-Kari, Pullen.

Note Added in Proof: The 14th author Jehrod B. Brenneman was accidentally left off the Fast Forward version of the article published December 6, 2022. The author list and affiliation list have been corrected.

References

An Y, Xu F, Le W, Ge Y, Zhou M, Chen H, Zeng C, Zhang H, and Liu Z (2015) Renal histologic changes and the outcome in patients with diabetic nephropathy. *Nephrol Dial Transplant* **30**:257–266.

Boustany-Kari CM, Harrison PC, Chen H, Lincoln KA, Qian HS, Clifford H, Wang H, Zhang X, Gueneva-Boucheva K, Bosanac T, et al. (2016) A Soluble Guanylate Cyclase Activator Inhibits the Progression of Diabetic Nephropathy in the ZSF1 Rat. *J Pharmacol Exp Ther* **356**:712–719.

Bénardeau A, Kahnert A, Schomber T, Meyer J, Pavkovic M, Kretschmer A, Lawrenz B, Hartmann E, Mathar I, Hueser J, et al. (2021) Runcaciguat, a novel soluble guanylate cyclase activator, shows renoprotection in hypertensive, diabetic, and metabolic preclinical models of chronic kidney disease. *Naunyn Schmiedebergs Arch Pharmacol* **394**:2363–2379.

Brenner BM, Cooper ME, de Zeeuw D, Keane WF, Mitch WE, Parving H-H, Remuzzi G, Snapinn SM, Zhang Z, and Shahinfar S; RENAAL Study Investigators (2001) Effects of losartan on renal and cardiovascular outcomes in patients with type 2 diabetes and nephropathy. *N Engl J Med* **345**:861–869.

Dellamea BS, Pinto LC, Leitão CB, Santos KG, and Canani LH (2014) Endothelial nitric oxide synthase gene polymorphisms and risk of diabetic nephropathy: a systematic review and meta-analysis. *BMC Med Genet* **15**:9.

Gewin LS (2018) Renal fibrosis: Primacy of the proximal tubule. *Matrix Biol* **68–69**:248–262.29425694

Gillis EE, Brinson KN, Rafikova O, Chen W, Musall JB, Harrison DG, and Sullivan JC (2018) Oxidative stress induces BH_4 deficiency in male, but not female, SHR. *Biosci Rep* **38**:BSR20180111.

Grgic I, Campanholle G, Bijol V, Wang C, Sabbisetti VS, Ichimura T, Humphreys BD, and Bonventre JV (2012) Targeted proximal tubule injury triggers interstitial fibrosis and glomerulosclerosis. *Kidney Int* **82**:172–183.

Hahn MG, Lampe T, El Sheikh S, Griebenow N, Woltering E, Schlemmer KH, Dietz L, Gerisch M, Wunder F, Becker-Pelster EM, et al. (2021). Discovery of the Soluble Guanylate Cyclase Activator Runcaciguat (BAY 1101042). *J Med Chem* **64**:5323–5344.

Hanai K, Babazono T, Nyumura I, Toya K, Tanaka N, Tanaka M, Ishii A, and Iwamoto Y (2009) Asymmetric dimethylarginine is closely associated with the development and progression of nephropathy in patients with type 2 diabetes. *Nephrol Dial Transplant* **24**:1884–1888.

Koye DN, Magliano DJ, Nelson RG, and Pavkov ME (2018) The Global Epidemiology of Diabetes and Kidney Disease. *Adv Chronic Kidney Dis* **25**:121–132.

Lajer M, Tarnow L, Jorsal A, Teerlink T, Parving H-H, and Rossing P (2008) Plasma concentration of asymmetric dimethylarginine (ADMA) predicts cardiovascular morbidity and mortality in type 1 diabetic patients with diabetic nephropathy. *Diabetes Care* **31**:747–752.

Lewis EJ, Hunsicker LG, Bain RP, and Rohde RD; The Collaborative Study Group (1993) The effect of angiotensin-converting-enzyme inhibition on diabetic nephropathy. *N Engl J Med* **329**:1456–1462.

Lewis EJ, Hunsicker LG, Clarke WR, Berl T, Pohl MA, Lewis JB, Ritz E, Atkins RC, Rohde R, and Raz I; Collaborative Study Group (2001) Renoprotective effect of the

angiotensin-receptor antagonist irbesartan in patients with nephropathy due to type 2 diabetes. *N Engl J Med* **345**:851–860.
Nagle RB, Bulger RE, Cutler RE, Jervis HR, and Benditt EP (1973) Unilateral obstructive nephropathy in the rabbit. I. Early morphologic, physiologic, and histochemical changes. *Lab Invest* **28**:456–467.
Nath KA (1992) Tubulointerstitial Changes as a Major Determinant in the Progression of Renal Damage. *American Journal of Kidney Diseases* **20**:1–17.
Nedvetsky PI, Kleinschnitz C, and Schmidt HHHW (2002) Regional distribution of protein and activity of the nitric oxide receptor, soluble guanylyl cyclase, in rat brain suggests multiple mechanisms of regulation. *Brain Res* **950**:148–154.
Persson F, Rossing P, Hovind P, Stehouwer CDA, Schalkwijk CG, Tarnow L, and Parving H-H (2008) Endothelial dysfunction and inflammation predict development of diabetic nephropathy in the Irbesartan in Patients with Type 2 Diabetes and Microalbuminuria (IRMA 2) study. *Scand J Clin Lab Invest* **68**:731–738.
Rianto F, Kuma A, Ellis CL, Hassounah F, Rodriguez EL, Wang XH, Sands JM, and Klein JD (2020) UT-A1/A3 knockout mice show reduced fibrosis following unilateral ureteral obstruction. *Am J Physiol Renal Physiol* **318**:F1160–F1166.
Stasch J-P, Becker EM, Alonso-Alija C, Apeler H, Dembowsky K, Feurer A, Gerzer R, Minuth T, Perzborn E, Pleiss U, et al. (2001) NO-independent regulatory site on soluble guanylate cyclase. *Nature* **410**:212–215.
Stasch J-P, Dembowsky K, Perzborn E, Stahl E, and Schramm M (2002) Cardiovascular actions of a novel NO-independent guanylyl cyclase stimulator, BAY 41-8543: *in vivo* studies. *Br J Pharmacol* **135**:344–355.
Stasch J-P, Schmidt PM, Nedvetsky PI, Nedvetskaya TY, H S AK, Meurer S, Deile M, Taye A, Knorr A, Lapp H, et al. (2006) Targeting the heme-oxidized nitric oxide receptor for selective vasodilatation of diseased blood vessels. *J Clin Invest* **116**:2552–2561.
Stasch J-P, Schlossmann J, and Hocher B (2015) Renal effects of soluble guanylate cyclase stimulators and activators: a review of the preclinical evidence. *Curr Opin Pharmacol* **21**:95–104.
Takaori K, Nakamura J, Yamamoto S, Nakata H, Sato Y, Takase M, Nameta M, Yamamoto T, Economides AN, Kohno K, et al. (2016) Severity and Frequency of Proximal Tubule Injury Determines Renal Prognosis. *J Am Soc Nephrol* **27**:2393–2406.
Tobin JV, Zimmer DP, Shea C, Germano P, Bernier SG, Liu G, Long K, Miyashiro J, Ranganath S, Jacobson S, et al. (2018) Pharmacological Characterization of IW-1973, a Novel Soluble Guanylate Cyclase Stimulator with Extensive Tissue Distribution, Antihypertensive, Anti-Inflammatory, and Antifibrotic Effects in Preclinical Models of Disease. *J Pharmacol Exp Ther* **365**:664–675.
Tuttle KR, Bakris GL, Bilous RW, Chiang JL, de Boer IH, Goldstein-Fuchs J, Hirsch IB, Kalantar-Zadeh K, Narva AS, Navaneethan SD, et al. (2014) Diabetic kidney disease: a report from an ADA Consensus Conference. *Diabetes Care* **37**:2864–2883.

Address correspondence to: Steven S. Pullen, Boehringer-Ingelheim Pharmaceuticals, 900 Ridgebury Road, PO Box 368, Ridgefield, CT 06877. E-mail: steven.pullen@boehringer-ingelheim.com

JPET-AR-2022-001423

Journal of Pharmacology and Experimental Therapeutics

The Novel, Clinical Stage Soluble Guanylate Cyclase Activator BI 685509 Protects from Disease Progression in Models of Renal Injury and Disease

Glenn A. Reinhart, Paul C. Harrison, Kathleen Lincoln, Hongxing Chen, Peng Sun, Jon Hill, Hu Sheng Qian, Mark C. McHugh, Holly Clifford, Joe Ng, Hong Wang, Danielle Fowler, Kristina Gueneva-Boucheva, Todd Bosanac, Diane Wong, Ryan M. Fryer, Chris Sarko, Carine M. Boustany-Kari, Steven S. Pullen

Cardiometabolic Diseases Research (G.A.R, P.C.H, K.L., H.C., P.S., H.Q., M.C.M., H.C., J.N., H.W., D.F., C.M.B.-K., S.S.P.), Small Molecule Discovery Research (K.G.-B., T.B., D.W., C.S.), Global Computational Biology and Data Sciences (J.H.)

Boehringer Ingelheim Pharmaceuticals, Inc, Ridgefield, CT.

Supplemental Methods

Telemetry Rat Blood Pressure and Heart Rate Profile

Rats were instrumented with DSI telemetry implants with catheters aseptically placed in the descending aorta as previously described (Fryer et al., 2012). Animals were single housed to record blood pressure and heart rate under conscious conditions.

Single Dose Study: BI 685509 was prepared as a nanosuspension in 1% Pluronic F127 in water and administered as single doses of 3, 10, and 30 mg/kg p.o. (5 mL/kg). Hemodynamic values were recorded for 8 hrs post-dose (n=8/group). A blood sample was withdrawn 8 hrs post-dose for analysis of drug plasma concentrations.

Repeat Dose Study: Following a baseline period, single-housed, drug-naïve telemetry-instrumented rats were randomized into 3 groups: Vehicle (0.5% methylcellulose and 0.015% Tween 80, 5 mL/kg) and BI 685509 at 60 or 100 mg/kg p.o., QD (n=12/group). Rats were treated for 10 consecutive days; on the 11^{th} day, all animals received a challenge dose of BI 685509 at 100 mg/kg p.o. to elicit a maximal hypotensive response and test potential for attenuation. Mean arterial pressure (MAP) and heart rate (HR) were collected continuously throughout the study. Analysis was based on calculating the maximal treatment-induced effect on MAP or HR following each daily dose; values were then averaged across each group and compared each day by one-way ANOVA with Dunnett's post-test vs. vehicle without adjusting for repeated measures.

Mouse PK: BI 685509 (suspended in 0.1% Tween and 0.5% Natrosol; 10 mL/kg) was administered as a single oral dose to male mice (5.83 mg/kg; n=3, B6.V-Lep-ob/J, Janvier Labs, Saint-Berthevin Cedex, France, 25g BW) under fed conditions. Blood samples (~25 µL) were collected into EDTA microtainers via retro-orbital sinus bleeds at the following timepoints (hrs) after dosing: 0, 0.25, 0.5, 1, 2, 4, 8, 24 and placed on ice for no longer than 30 minutes prior to centrifugation at 8000 rpm for 5 minutes. Following centrifugation, plasma samples were immediately transferred to Eppendorf tubes and stored frozen at -80°C prior to analysis. Plasma concentrations of BI 685509 were measured by LC-MS/MS as described below.

Rat PK: Male rats (n=3/ group, Wistar-Han, Charles River, Raleigh, NC, ~220-230 g BW) were administered a single intravenous (i.v.) or oral dose of BI 685509 under fasted conditions. For i.v. group, BI 685509 was dissolved in 70% PEG 400/30% water and administered as a bolus injection via the femoral cannula at 1 mg/kg (2 mL/kg). For the oral (p.o.) group, BI 685509 was administered as a suspension in 0.5% methyl cellulose/0.015% Tween 80 at 3 mg/kg (5 mL/kg). Blood samples (~200 µL into 1.5 mL polypropylene tubes with prefilled 10 µL 2M citric acid and 23 µL of sodium citrate) were collected via an indwelling jugular catheter at the following timepoints (hrs) after i.v. and p.o. dosing: 0, 0.25, 0.5, 1, 2, 4, 6, 8, 24 and an additional 0.083 hr timepoint was collected after i.v. administration. Following centrifugation, a 100 µL plasma sample was recovered and stored frozen at -40°C until analysis. Plasma concentrations of BI 685509 were measured by LC-MS/MS.

Pharmacokinetic Measurements

Following centrifugation (930 rcf for 10 min), urine samples were diluted in 0.1 N NaOH and protein concentration was determined using Coomassie Plus Reagent (Thermo Fisher, Waltham, MA, #23238).

The quantitation of enalaprilat and BI 685509 in heparin plasma and kidney cortex was performed via liquid chromatography/mass spectrophotometry (LC/MS/MS). An API 5000 triple quadruple mass spectrometer with Turbo V Ion Source (Applied Biosystems, Toronto, Canada), set to electrospray positive ionization mode, and Analyst 1.4.2 operating software was used. Ion transitions used for quantification were: enalaprilat (349.0-206.0 m/z, CE 25, DP 80V) and BI 685509 (583.2-244.2 m/z, CE 22, DP 80V). The liquid chromatography system was an Agilent 1200 Series pump and column oven (Fullerton, CA, USA) with a LEAP Technologies HTS-PAL Autosampler (Carrboro, NC, US). The analytical column was a Phenomenex Synergi Polar RP, 2.1 x 50 mm, 4 mm (Torrance, CA, US), and the mobile phase consisted of 0.1% formic acid in water (A) and 0.1 formic acid in Acetonitrile (B). Gradient was maintained at 5%B for 0.1 minute, increased to 95% B in 1.8 minutes, held at 95% B for 0.5 minute and decreased to 5% B for 0.2 minute and held at 5% B for a total time of 3 minutes at a flow rate of 0.5 ml/min. The total run time per injection was 3 minutes.

Sample Preparation: Enalaprilat and BI 685509 standard stock solutions containing 1 mg/mL in methanol were serially diluted in rat plasma to prepare an 8- point standard curve ranging from 1 to 5000 ng/mL. 20 μL of plasma, calibration standards and blank plasma samples were deproteinized by precipitation with 180 mL of internal standard (100 ng/mL; proprietary small molecule) diluted in acetonitrile: water (85:15). Samples were mixed for 1 min, filtered through AcroPrep Multi-well filter plates (Pall Corporation, Ann Arbor,

MI) using Sciclone ALH 3000 Workstation (Caliper Life Sciences, Hopkinton, MA, USA) and transferred into 96-well injection plate. 5 mL of the solution was then injected into the LC/MS/MS system for analysis.

HbA1c was measured by high-pressure liquid chromatography (DTI Laboratories, Thomasville, GA). Fasting plasma glucose was measured utilizing a glucose meter (Bayer Breeze2; Bayer HealthCare LLC, Mishawaka, IN).

Pharmacokinetics/Pharmacodynamics (PK/PD) modeling

Overall change from baseline in UPE across the study was correlated with BI 685509 individual mean plasma concentrations using an inhibitory effect I_{max} model. All analyses were performed using Phoenix WinNonlin Version 6.1 (Pharsight, Cary, NC).

Tissue Collection and Processing

For histological assessment, kidneys were removed, weighed and a mid-organ transverse section of the left kidney was collected and immediately fixed by immersion in 10% phosphate-buffered formalin for 48 hrs. Subsequently, formalin-fixed tissues were washed in phosphate buffer, dehydrated through a graded series of ethanol and xylene, embedded in paraffin, and sectioned at 4 µm.

General Assessment of Renal Histopathology

Kidney tissue sections (4 µm) were stained with periodic acid methenamine silver (PAM) for the general assessment of incidence of glomerulosclerosis and hematoxylin–eosin (H&E) for the general assessment of total number of foci of interstitial lesions. For the

glomerular lesions, the number of glomeruli showing mild to severe glomerulosclerosis were counted in each kidney section and expressed as a percentage of the total glomerular population. Tubulointerstitial lesions were assessed as the number of foci showing obvious renal damage, which included marked hypercellularity (inflammation or resident myofibroblast increases), fibrosis, tubular hyperplasia, casts, or necrosis. Both assessments were performed under blinded conditions at 10X magnification.

Immunohistochemistry and Image Analysis

Four micrometer kidney sections were air dried overnight at 37°C, dewaxed and rehydrated in graded ethanol to phosphate buffered saline (PBS). Endogenous peroxidase activity was blocked by ImmPRESS (Vector Laboratories, Burlingame, CA) for 20 min at ambient temperature. Sections were then washed and incubated with the primary antibody for α-smooth muscle actin (α-SMA; A5228, Sigma, St. Louis, MO) at a dilution of 1:3000, kidney injury molecule-1 (KIM-1; AF3689, R&D Systems, Minneapolis, MN) at a dilution of 1:200 and the rat cellular marker for microglia, monocytes and macrophages (ED-1, MAB1435, Millipore, Temecula, CA) at a dilution of 1:80, and were subsequently incubated with the respective secondary antibodies (ImmPress Reagent Kit, Vector Laboratory, Burlingame, CA) for 30 minutes in a hydration chamber. Immunoperoxidase detection was performed using the avidin-biotin complex method (Vector Laboratories, Burlingame, CA) using 3, 3′-diaminobenzidine tetra hydrochloride as substrate.

Quantitative image analysis of α-SMA, KIM-1 and ED-1 staining was performed under blinded conditions. Ten random digital images were captured at 10X objective magnification, with each field representing approximately 0.6 mm^2 for a total area of 6.0 mm^2 being

assessed. The percentage of positive staining area per field in the cortex region was measured using computer assisted image analysis with Image-Pro imaging software.

NGS: Sequencing libraries were built according to the manufacturer's procedures for the TruSeq polyA kit. Sequencing was performed on an Illumina HiSeq 2500 to a depth ranging from 17 to 25 million reads, with a read length of 50 bases (N=7 for sham and N=9 for drug treated).

The sequencing data were mapped to the reference genome Rnor_6.0 using the STAR aligner (Dobin 2013). Gene quantitation was performed with RSEM for generation of TPM and feature counts for generation of counts used in downstream analysis. Principal component analysis was used to assess overall sample similarity.

Differential gene expression analysis was performed first independently on the two doses each compared to the vehicle-treated group, using the voom-limma method (Law, 2014). The two doses had a high-degree of overall concordance (Suppl. Fig. 3), so the analysis was repeated by pooling the two dose conditions and comparing them to the vehicle-treated group. This analysis resulted in a list of differentially expressed genes presented in Suppl. Table 5, based on a threshold using a false discovery rate (FDR) threshold of less than 0.05 for statistical significance and a threshold of fold change between groups of ± 2.

Supplemental Table 1. Mean plasma concentration of BI 685509 after oral administration of 5.83 mg/kg BI 685509 in B6.V-Lep-ob/J mice

Time (Hr)	Plasma Concentration (nM)
0.25	866 ± 82.2
0.5	510 ± 41.9
1	296 ± 29.7
2	165 ± 27.1
4	120 ± 14.2
8	79.1 ± 19.2
24	1.74 ± 0.415

Plasma levels reported as mean ± SEM in nM for BI 685509

Supplemental Table 2. Mean plasma concentration of BI 685509 afteri.v. 1 mg/kg and oral 3 mg/kg administration of BI 685509 in wistar han rats

Time (Hr)	Plasma Concentration (nM)	
	IV	PO
0.0833	1920 ± 123	-
0.25	-	606 ± 71.6
0.5	346 ± 84.3	502 ± 120
1	94.7 ± 22.1	338 ± 73.9
2	27.9 ± 1.94	297 ± 68.1
4	5.48 ± 1.31	162 ± 45.4
6	5.71 ± 1.17	72.0 ± 23.8
8	1.88 ± 0.98	28.2 ± 10.4
24	0	0.612 ± 0.61

Plasma levels reported as mean ± SEM in nM for BI 685509

Supplemental Table 3

Ensg	Symbol	Log2FoldChange	P.Value	Adj.P.Val
ENSRNOG00000016753	Slc14a1	-2.1	2.97E-14	4.67E-10
ENSRNOG00000004030	Nphs2	1.24	4.30E-13	2.25E-09
ENSRNOG00000033609	Irx1	-1.06	1.73E-12	6.80E-09
ENSRNOG00000054360	Tspan11	-1.04	1.53E-11	3.43E-08
ENSRNOG00000061890	Ust5r	-1.35	1.96E-11	3.86E-08
ENSRNOG00000011861	Aadat	-1.7	3.97E-11	5.67E-08
ENSRNOG00000007290	Atp1a2	-1.17	4.80E-11	6.29E-08
ENSRNOG00000009514	Mme	-1.12	1.00E-10	9.84E-08
ENSRNOG00000010388	Slc21a4	-1.73	1.39E-10	1.29E-07
ENSRNOG00000039596	Prob1	-1.05	1.53E-10	1.34E-07
ENSRNOG00000045743	Etnppl	-2.18	1.89E-10	1.48E-07
ENSRNOG00000004018	Tdrd5	1.4	2.53E-10	1.81E-07
ENSRNOG00000030894	Slco1a6	-2.05	2.61E-10	1.81E-07
ENSRNOG00000003616	Grem2	-2.3	4.52E-10	2.67E-07
ENSRNOG00000018420	Slc22a7	-2.13	4.80E-10	2.67E-07
ENSRNOG00000006302	Gclc	-1.51	4.92E-10	2.67E-07
ENSRNOG00000057855	F5	-1.04	5.47E-10	2.78E-07
ENSRNOG00000025848	Sspo	-1.96	6.33E-10	3.11E-07
ENSRNOG00000007932	Gcm1	-2.11	6.55E-10	3.12E-07
ENSRNOG00000018266	Slc23a3	-1.38	7.66E-10	3.43E-07
ENSRNOG00000001159	Tff3	-1.82	8.54E-10	3.53E-07
ENSRNOG00000021771	Trim29	-1.79	8.90E-10	3.58E-07
ENSRNOG00000061695	Slc23a1	-1.07	1.79E-09	6.28E-07
ENSRNOG00000000158	Cdo1	-1.35	1.82E-09	6.28E-07

ENSRNOG00000018445	Agt	-1.45	1.84E-09	6.28E-07
ENSRNOG00000016625	Slc22a2	-1.24	2.43E-09	7.79E-07
ENSRNOG00000005223	Hnmt	-2.14	2.48E-09	7.79E-07
ENSRNOG00000025648	Dhrs7l1	-1.93	2.61E-09	7.88E-07
ENSRNOG00000014948	Osgin1	-1.18	2.70E-09	8.02E-07
ENSRNOG00000057904	LOC102554608	-2.6	4.22E-09	1.16E-06
ENSRNOG00000003620	Fmo3	-1.17	4.37E-09	1.18E-06
ENSRNOG00000028889	Slc51b	-1.24	4.58E-09	1.22E-06
ENSRNOG00000033581	Tnxb	-1	5.04E-09	1.28E-06
ENSRNOG00000057557	Prlr	-1.16	5.30E-09	1.28E-06
ENSRNOG00000012843	Aspg	-1.09	5.38E-09	1.28E-06
ENSRNOG00000015461	Serpine2	-1.01	5.82E-09	1.34E-06
ENSRNOG00000015089	Mcoln2	-1.57	7.34E-09	1.65E-06
ENSRNOG00000004795	Pof1b	-2.46	7.51E-09	1.66E-06
ENSRNOG00000007590	Eya1	-1.03	1.03E-08	2.13E-06
ENSRNOG00000059790	Krt78	-2.33	1.15E-08	2.28E-06
ENSRNOG00000017672	Akr1c14	-1.35	1.42E-08	2.76E-06
ENSRNOG00000009440	Gucy1b2	-1.91	2.41E-08	4.56E-06
ENSRNOG00000050714	Islr2	1.63	2.44E-08	4.56E-06
ENSRNOG00000012575	Fat2	-2.18	4.66E-08	7.94E-06
ENSRNOG00000024903	Slc7a13	-2.14	4.70E-08	7.94E-06
ENSRNOG00000004958	Slc22a22	-1.6	4.85E-08	8.11E-06
ENSRNOG00000033266	Prss30	-1.14	5.87E-08	9.41E-06
ENSRNOG00000016827	Slc38a3	-1.52	8.48E-08	1.26E-05
ENSRNOG00000022711	Slco4c1	-1.41	8.48E-08	1.26E-05
ENSRNOG00000009797	Aqp3	-1.04	1.29E-07	1.75E-05
ENSRNOG00000006120	Shh	-1.54	1.53E-07	1.92E-05

ENSRNOG00000003119	Gc	-1.52	1.64E-07	2.00E-05
ENSRNOG00000019467	Fer1l4	-2.29	1.81E-07	2.14E-05
ENSRNOG00000054378	Aqp2	-1.36	1.86E-07	2.16E-05
ENSRNOG00000025501	Snx31	-2.16	2.43E-07	2.71E-05
ENSRNOG00000007949	Rgn	-1.6	2.66E-07	2.90E-05
ENSRNOG00000029179	Cyp2d1	-1.13	2.85E-07	3.03E-05
ENSRNOG00000007980	Anxa13	-1.63	2.92E-07	3.06E-05
ENSRNOG00000034087	Krt42	-2.1	2.96E-07	3.08E-05
ENSRNOG00000003288	Cacng5	-2.34	3.23E-07	3.27E-05
ENSRNOG00000013704	Cps1	-1.57	3.53E-07	3.47E-05
ENSRNOG00000027739	Cndp1	-1.08	4.22E-07	4.06E-05
ENSRNOG00000027380	Upk1b	-2.31	4.48E-07	4.29E-05
ENSRNOG00000004828	Acvr1c	-1.08	5.58E-07	5.18E-05
ENSRNOG00000022767	Elfn1	-1.12	5.64E-07	5.19E-05
ENSRNOG00000015902	Cpxm2	-1.33	5.73E-07	5.24E-05
ENSRNOG00000009388	Sptssb	-2.8	5.76E-07	5.24E-05
ENSRNOG00000019445	Msln	-1.76	5.96E-07	5.35E-05
ENSRNOG00000025059	Nxph4	-1.42	6.16E-07	5.48E-05
ENSRNOG00000024331	Upk1a	-2.32	6.97E-07	6.12E-05
ENSRNOG00000060681	LOC102553472	1.84	1.12E-06	9.40E-05
ENSRNOG00000017786	Acta1	-1.65	1.18E-06	9.70E-05
ENSRNOG00000058571	N/A	-1.46	1.22E-06	1.00E-04
ENSRNOG00000024028	Sprr1a	-2.61	1.58E-06	1.25E-04
ENSRNOG00000021095	Fxyd3	-2.38	1.67E-06	1.30E-04
ENSRNOG00000053494	Mcpt1l1	-2.84	1.87E-06	1.43E-04
ENSRNOG00000010805	Fabp4	-1.78	1.91E-06	1.45E-04
ENSRNOG00000036984	Slco1a1	-2.02	2.14E-06	1.58E-04

ENSRNOG00000031263	Haao	-1.08	2.26E-06	1.66E-04
ENSRNOG00000054508	Foxp2	-1.49	2.30E-06	1.67E-04
ENSRNOG00000029401	Actg2	-1.84	2.48E-06	1.75E-04
ENSRNOG00000016325	F2	-1.24	2.68E-06	1.87E-04
ENSRNOG00000011808	Ghrhr	-1.22	2.93E-06	2.02E-04
ENSRNOG00000000961	Glt1d1	-1.41	2.99E-06	2.05E-04
ENSRNOG00000015682	Kel	1.1	3.10E-06	2.12E-04
ENSRNOG00000029427	Grhl3	-1.39	3.25E-06	2.19E-04
ENSRNOG00000060067	LOC102549636	-1.44	3.44E-06	2.30E-04
ENSRNOG00000050243	Akr1c12l1	-1.29	3.47E-06	2.31E-04
ENSRNOG00000012720	Irx4	-1.2	3.59E-06	2.37E-04
ENSRNOG00000060949	Anxa8	-2.58	3.88E-06	2.44E-04
ENSRNOG00000009314	Ivl	-2.29	3.97E-06	2.46E-04
ENSRNOG00000017872	LOC688778	-2.2	3.97E-06	2.46E-04
ENSRNOG00000056555	N/A	-1.64	4.19E-06	2.56E-04
ENSRNOG00000008015	Fos	1.14	4.41E-06	2.68E-04
ENSRNOG00000006962	Stk32c	-1.57	4.54E-06	2.72E-04
ENSRNOG00000053746	Olr1668	-3.73	4.57E-06	2.73E-04
ENSRNOG00000037080	Adamts17	-1.17	6.50E-06	3.64E-04
ENSRNOG00000033490	Vsig2	-1.81	6.88E-06	3.79E-04
ENSRNOG00000019500	Cyp1a1	-2.97	6.93E-06	3.80E-04
ENSRNOG00000049345	Mep1b	-1.43	9.83E-06	5.07E-04
ENSRNOG00000024899	Cxcl13	1.22	1.05E-05	5.34E-04
ENSRNOG00000004564	Lrriq1	-1.09	1.06E-05	5.39E-04
ENSRNOG00000013593	Upk3a	-2.86	1.08E-05	5.44E-04
ENSRNOG00000054016	N/A	-2.2	1.09E-05	5.47E-04
ENSRNOG00000029964	Tmprss11g	-1.96	1.10E-05	5.53E-04

ENSRNOG00000054957	Sfrp4	-1.43	1.11E-05	5.55E-04
ENSRNOG00000056396	N/A	-1.55	1.17E-05	5.76E-04
ENSRNOG00000003566	Apoh	-1.44	1.21E-05	5.83E-04
ENSRNOG00000000383	Mypn	-1.65	1.22E-05	5.90E-04
ENSRNOG00000032002	Hapln1	-1.57	1.26E-05	6.00E-04
ENSRNOG00000001967	Sult1b1	-1	1.34E-05	6.26E-04
ENSRNOG00000023497	Foxe1	-1.5	1.37E-05	6.33E-04
ENSRNOG00000013036	Epha8	-1.71	1.38E-05	6.34E-04
ENSRNOG00000029128	Cyp2d5	-1.64	1.44E-05	6.54E-04
ENSRNOG00000023686	Upk3b	-1.04	1.80E-05	7.88E-04
ENSRNOG00000011381	Acsbg1	-1.67	1.96E-05	8.49E-04
ENSRNOG00000060413	N/A	-1.69	2.10E-05	8.91E-04
ENSRNOG00000022116	Gjb6	-2.23	2.36E-05	9.67E-04
ENSRNOG00000029911	Cilp	-1.11	2.52E-05	1.03E-03
ENSRNOG00000003899	Krt14	-2.24	2.60E-05	1.05E-03
ENSRNOG00000023561	Ano2	-1.81	2.79E-05	1.11E-03
ENSRNOG00000001691	Cldn14	1.6	2.91E-05	1.14E-03
ENSRNOG00000012906	Bcas1	-1.77	3.34E-05	1.26E-03
ENSRNOG00000042330	Ms4a18	1.4	3.35E-05	1.26E-03
ENSRNOG00000037960	LOC689499	-1.19	3.38E-05	1.26E-03
ENSRNOG00000043324	Upk2	-2.55	3.42E-05	1.27E-03
ENSRNOG00000059314	N/A	-1.35	3.75E-05	1.37E-03
ENSRNOG00000003740	Gpa33	-1.77	3.81E-05	1.39E-03
ENSRNOG00000001984	Kcne1	1.11	4.16E-05	1.50E-03
ENSRNOG00000014099	Krt15	-2.59	4.31E-05	1.55E-03
ENSRNOG00000054898	N/A	-1.97	5.19E-05	1.78E-03
ENSRNOG00000019685	Gdpd3	-1.46	5.60E-05	1.89E-03

ENSRNOG00000009160	N/A	-2.08	6.24E-05	2.08E-03
ENSRNOG00000002640	Serpinb5	-1.45	6.59E-05	2.18E-03
ENSRNOG00000010685	Tbx18	-1.61	7.50E-05	2.40E-03
ENSRNOG00000032871	Mlc1	-1.94	7.59E-05	2.42E-03
ENSRNOG00000060281	N/A	-1.54	7.75E-05	2.46E-03
ENSRNOG00000010031	Vtn	-1.05	7.87E-05	2.49E-03
ENSRNOG00000009284	Foxa1	-1.39	8.23E-05	2.58E-03
ENSRNOG00000037171	Tdgf1	1.74	8.48E-05	2.62E-03
ENSRNOG00000014314	Slc39a4	1.04	9.04E-05	2.77E-03
ENSRNOG00000011706	Mbl1	-1.89	9.26E-05	2.82E-03
ENSRNOG00000029514	Slc26a9	1.07	9.30E-05	2.82E-03
ENSRNOG00000012566	Kcnv2	-1.33	1.00E-04	2.98E-03
ENSRNOG00000009052	Igf2bp3	-1.07	1.01E-04	3.01E-03
ENSRNOG00000034031	Vstm2l	1.15	1.02E-04	3.01E-03
ENSRNOG00000005858	Kap	-1.14	1.12E-04	3.22E-03
ENSRNOG00000007335	Ccl11	-1.47	1.17E-04	3.34E-03
ENSRNOG00000004278	Dlx3	1.02	1.22E-04	3.46E-03
ENSRNOG00000001924	Tp63	-1.86	1.26E-04	3.54E-03
ENSRNOG00000009239	Entpd8	-1.33	1.26E-04	3.54E-03
ENSRNOG00000032959	Adh7	-1.76	1.28E-04	3.59E-03
ENSRNOG00000011575	Adamts18	1.6	1.49E-04	4.03E-03
ENSRNOG00000008219	Ccdc33	1.09	1.56E-04	4.17E-03
ENSRNOG00000050860	Abcb11	-1.55	1.64E-04	4.35E-03
ENSRNOG00000015716	Gp2	-1.06	1.73E-04	4.48E-03
ENSRNOG00000050420	Krt5	-3.01	1.91E-04	4.89E-03
ENSRNOG00000056021	Slc14a2	-2.63	1.94E-04	4.94E-03
ENSRNOG00000053631	Tdrd9	-1.14	1.97E-04	4.99E-03

ENSRNOG00000029147	Rbm11	1.36	2.03E-04	5.07E-03
ENSRNOG00000028985	LOC361914	-1.95	2.22E-04	5.43E-03
ENSRNOG00000010834	Mpped1	-1.02	2.25E-04	5.47E-03
ENSRNOG00000000963	Tmem132c	-1.46	2.44E-04	5.84E-03
ENSRNOG00000000428	Cyp21a1	-1.08	2.51E-04	5.94E-03
ENSRNOG00000011132	LOC100362814	-1.08	2.63E-04	6.14E-03
ENSRNOG00000004062	C4bpa	-1.01	2.68E-04	6.21E-03
ENSRNOG00000016243	Casq2	-1.17	2.82E-04	6.50E-03
ENSRNOG00000055888	N/A	-1.72	3.11E-04	7.05E-03
ENSRNOG00000046260	LOC688320	-2.19	3.96E-04	8.40E-03
ENSRNOG00000037982	Tmem236	-1.22	4.92E-04	9.93E-03
ENSRNOG00000057928	N/A	-3.57	4.98E-04	9.97E-03
ENSRNOG00000021735	Akr1cl	-1.08	5.21E-04	1.02E-02
ENSRNOG00000031569	Zfp648	-1.64	5.39E-04	1.05E-02
ENSRNOG00000008353	Iqch	-1.1	5.44E-04	1.05E-02
ENSRNOG00000042581	Ptcra	-1.09	6.17E-04	1.15E-02
ENSRNOG00000014296	Syt10	-1.57	6.60E-04	1.21E-02
ENSRNOG00000021796	RGD1565166	-1.59	7.49E-04	1.33E-02
ENSRNOG00000026060	Arsi	-1.03	7.50E-04	1.33E-02
ENSRNOG00000024259	Tmem54	-1.29	7.65E-04	1.35E-02
ENSRNOG00000028473	LOC691551	-1.47	8.55E-04	1.48E-02
ENSRNOG00000059050	Gm5414	-1.68	8.63E-04	1.48E-02
ENSRNOG00000046403	RGD1564999	-1.47	8.74E-04	1.50E-02
ENSRNOG00000020998	Oosp1	-1.13	9.06E-04	1.54E-02
ENSRNOG00000030285	Epha3	-1.18	9.40E-04	1.57E-02
ENSRNOG00000032669	Serpina1	-1.22	9.77E-04	1.61E-02
ENSRNOG00000002937	Ren	1.12	9.99E-04	1.62E-02

ENSRNOG00000001777	N/A	-1.22	1.00E-03	1.62E-02
ENSRNOG00000047046	Plin4	-1.28	1.10E-03	1.74E-02
ENSRNOG00000014231	Pnoc	-1.47	1.13E-03	1.77E-02
ENSRNOG00000057198	N/A	-1.21	1.22E-03	1.86E-02
ENSRNOG00000028082	Tal2	-1.06	1.23E-03	1.87E-02
ENSRNOG00000012404	Thrsp	-1.27	1.28E-03	1.92E-02
ENSRNOG00000002350	Eaf2	-1.1	1.30E-03	1.94E-02
ENSRNOG00000012557	Lgals5	1.36	1.30E-03	1.95E-02
ENSRNOG00000027506	Zp4	1.36	1.32E-03	1.96E-02
ENSRNOG00000005336	Prss27	-1.27	1.46E-03	2.10E-02
ENSRNOG00000008478	Mmp13	-1.39	1.57E-03	2.23E-02
ENSRNOG00000004067	Nrcam	1.07	1.58E-03	2.23E-02
ENSRNOG00000015518	Rbp4	-1.79	1.68E-03	2.34E-02
ENSRNOG00000010454	Ccno	-1.24	1.73E-03	2.39E-02
ENSRNOG00000054457	N/A	1.02	1.77E-03	2.43E-02
ENSRNOG00000039279	Nhlrc4	1.35	1.77E-03	2.43E-02
ENSRNOG00000046235	LOC686967	-1.74	1.79E-03	2.45E-02
ENSRNOG00000053334	Stmn4	1.17	1.80E-03	2.46E-02
ENSRNOG00000017198	Hif3a	-1.16	1.85E-03	2.49E-02
ENSRNOG00000055499	Grid1	-1.44	1.90E-03	2.54E-02
ENSRNOG00000033830	Slc7a12	-1.3	2.00E-03	2.61E-02
ENSRNOG00000025235	Tmem130	1.1	2.17E-03	2.74E-02
ENSRNOG00000060511	Tcap	-1.17	2.18E-03	2.75E-02
ENSRNOG00000016311	Slc6a2	-1.44	2.21E-03	2.77E-02
ENSRNOG00000011824	Trh	1.24	2.27E-03	2.82E-02
ENSRNOG00000026577	Cpne4	-1.36	2.32E-03	2.87E-02
ENSRNOG00000023397	LOC100911104	-2.31	2.40E-03	2.95E-02

ENSRNOG00000060524	N/A	-1.18	2.48E-03	3.01E-02
ENSRNOG00000059540	Gcnt3	-1.09	2.53E-03	3.05E-02
ENSRNOG00000025037	Ankk1	-1.39	2.63E-03	3.13E-02
ENSRNOG00000032508	Acot5	-1.15	2.63E-03	3.13E-02
ENSRNOG00000060211	N/A	1.1	2.72E-03	3.17E-02
ENSRNOG00000015477	Nkx3-1	1.35	3.19E-03	3.54E-02
ENSRNOG00000008337	Gjd2	-1.32	3.27E-03	3.59E-02
ENSRNOG00000015799	LOC103690120	-1.24	3.29E-03	3.61E-02
ENSRNOG00000061299	LOC100134871	1.07	3.40E-03	3.66E-02
ENSRNOG00000033588	Siglec15	-1.34	3.47E-03	3.71E-02
ENSRNOG00000002134	LOC103690086	-1.48	3.90E-03	4.02E-02
ENSRNOG00000053703	N/A	-1.41	4.11E-03	4.19E-02
ENSRNOG00000015086	Plin1	-2	4.11E-03	4.19E-02
ENSRNOG00000060975	N/A	-1.09	4.33E-03	4.35E-02
ENSRNOG00000058442	N/A	-1.33	4.87E-03	4.71E-02
ENSRNOG00000001001	Retn	-1.39	4.94E-03	4.75E-02

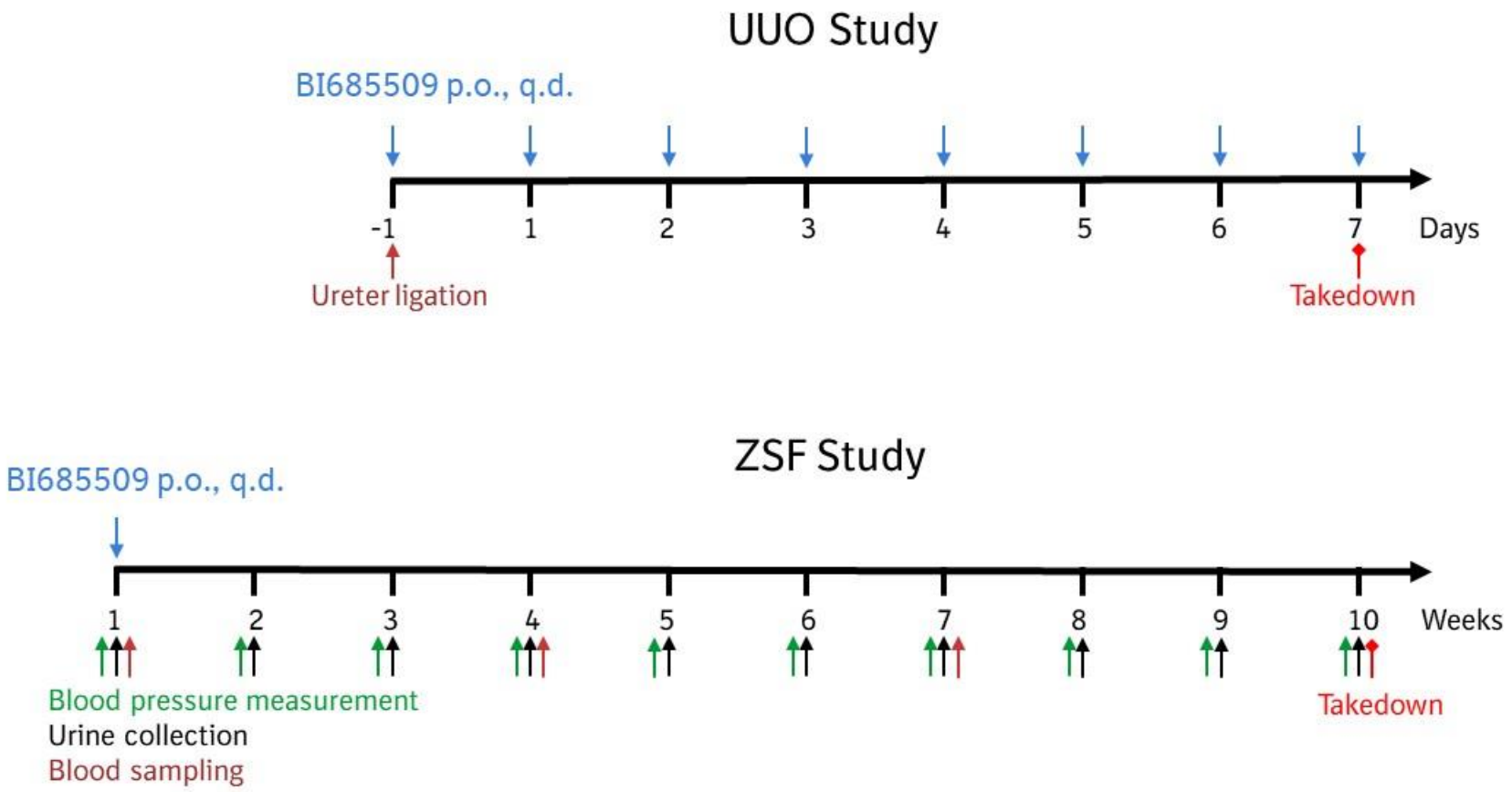

Supplemental Fig. 1. General study protocol for UUO and ZSF1 studies indicating relative time for procedures during the course of the 7d or 10wk studies, respectively.

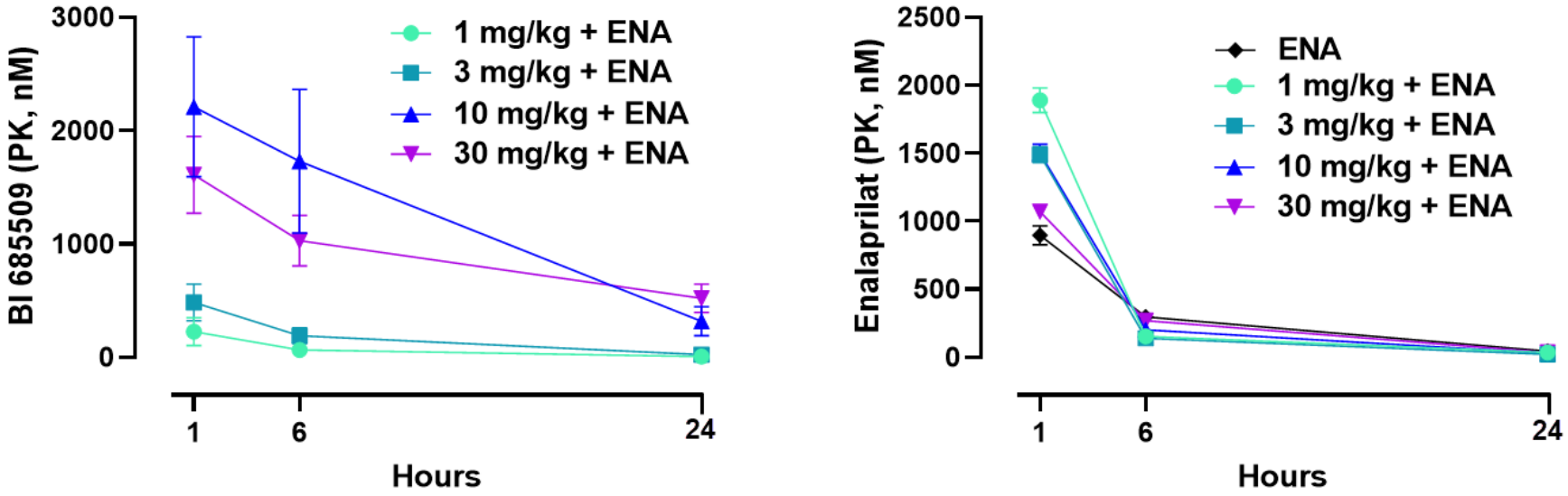

Supplemental Fig. 2. Mean plasma concentrations of BI 685509 (A) and enalaprilat (B) in ZSF1 rats. Plasma levels reported as mean ± SEM in nM by averaging the timepoints for weeks 1, 4, 7 and 10 per group.

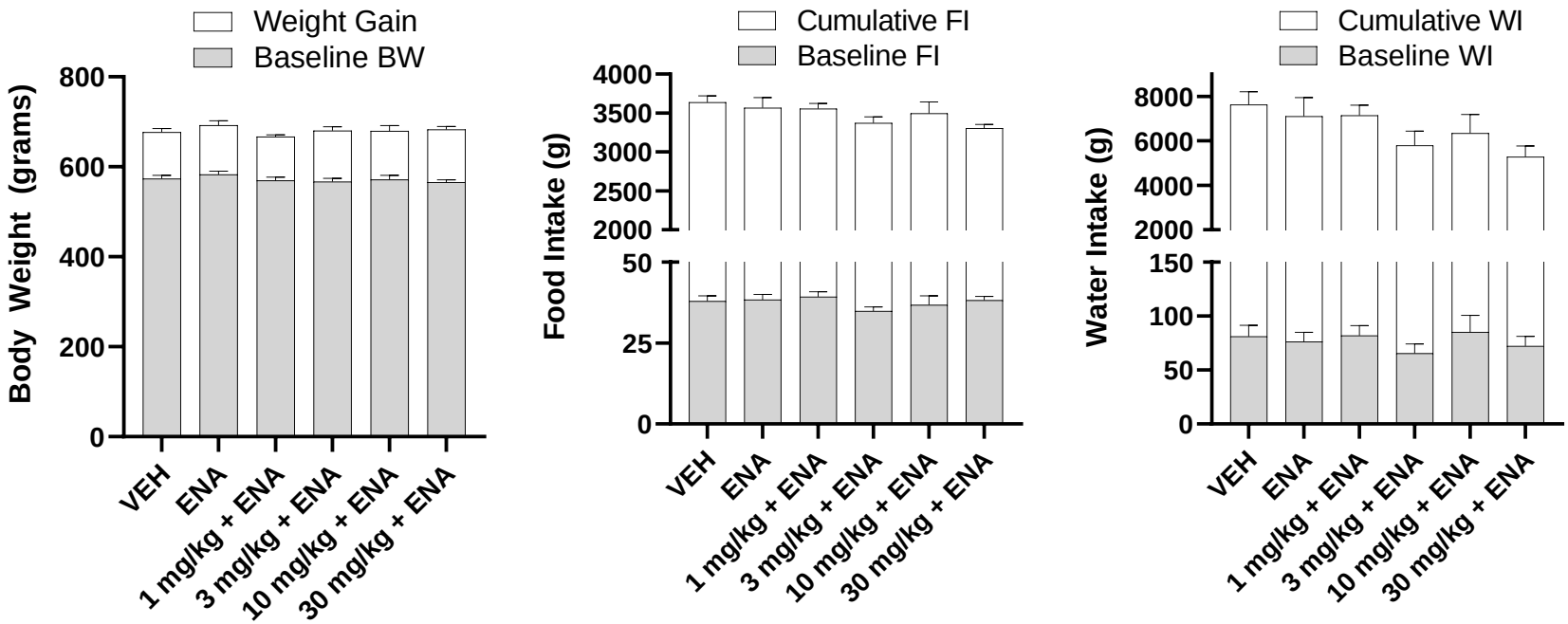

Supplemental Fig 3: Effects of BI 685509 and enalapril on body weight and feeding parameters. Parameters of body weight, food intake and water intake shown at baseline (Day 0) and following 10 weeks of treatment. There were no significant differences in these parameters between study groups (one way ANOVA vs. vehicle or enalapril treated groups, Dunnett's post-test).

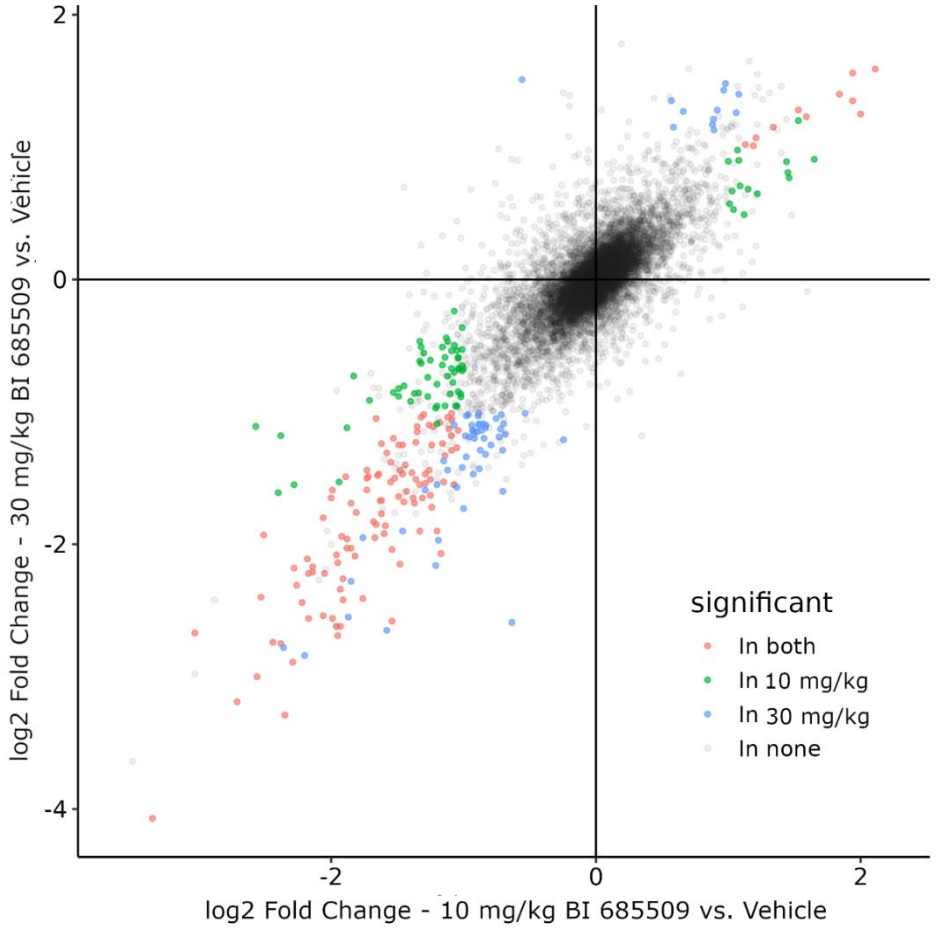

Supplemental Fig. 4. Scatterplot of changes of fold-change between BI 685509 and Vehicle-treated groups in UUO model, comparing 10 mg/kg and 30 mg/kg doses.

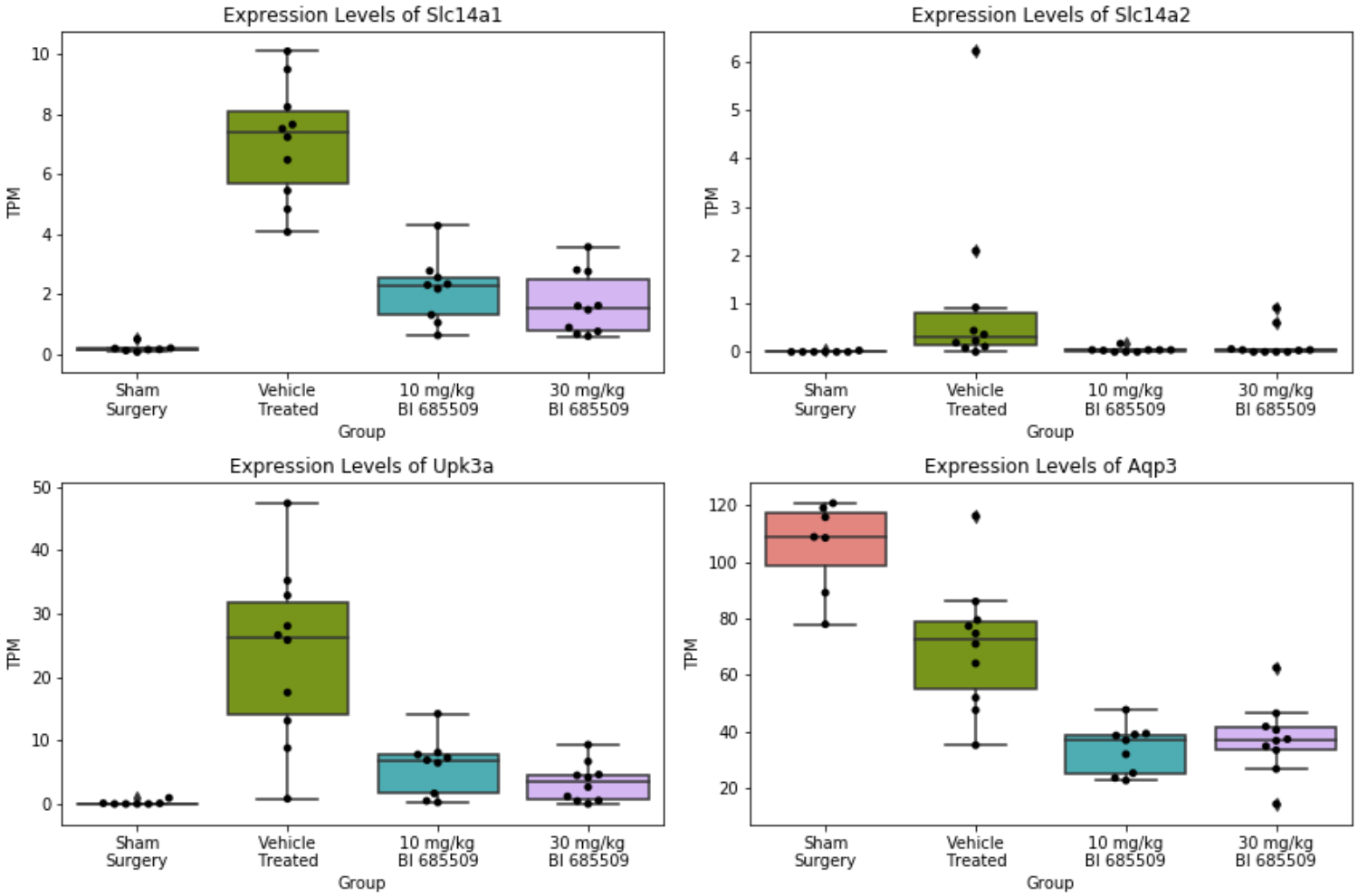

Supplemental Fig. 5. Boxplots of gene expression across groups for urate transporters, Slc14a1, Slc14a2, Upk3a, and Aqp3.

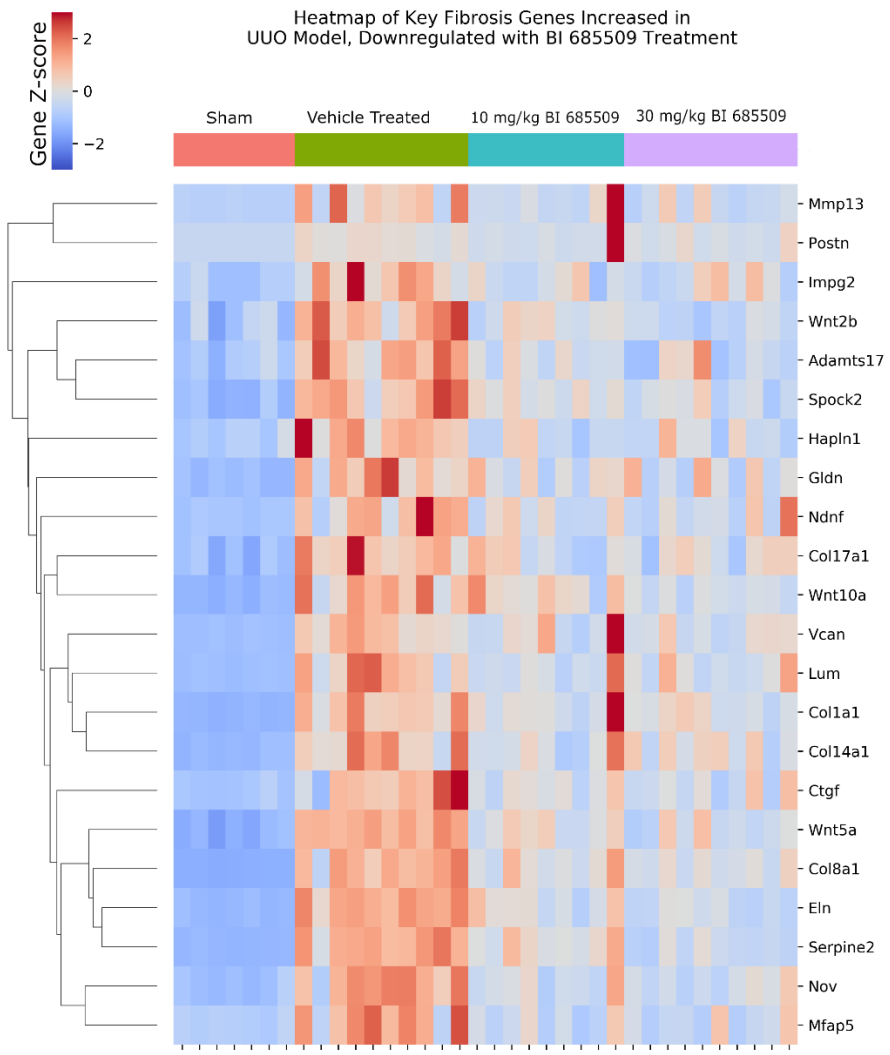

Supplemental Fig. 6. Heatmap of extracellular-matrix-associated genes upregulated in UUO model and downregulated in groups treated with 10 mg/kg and 30 mg/kg doses of BI 685509.

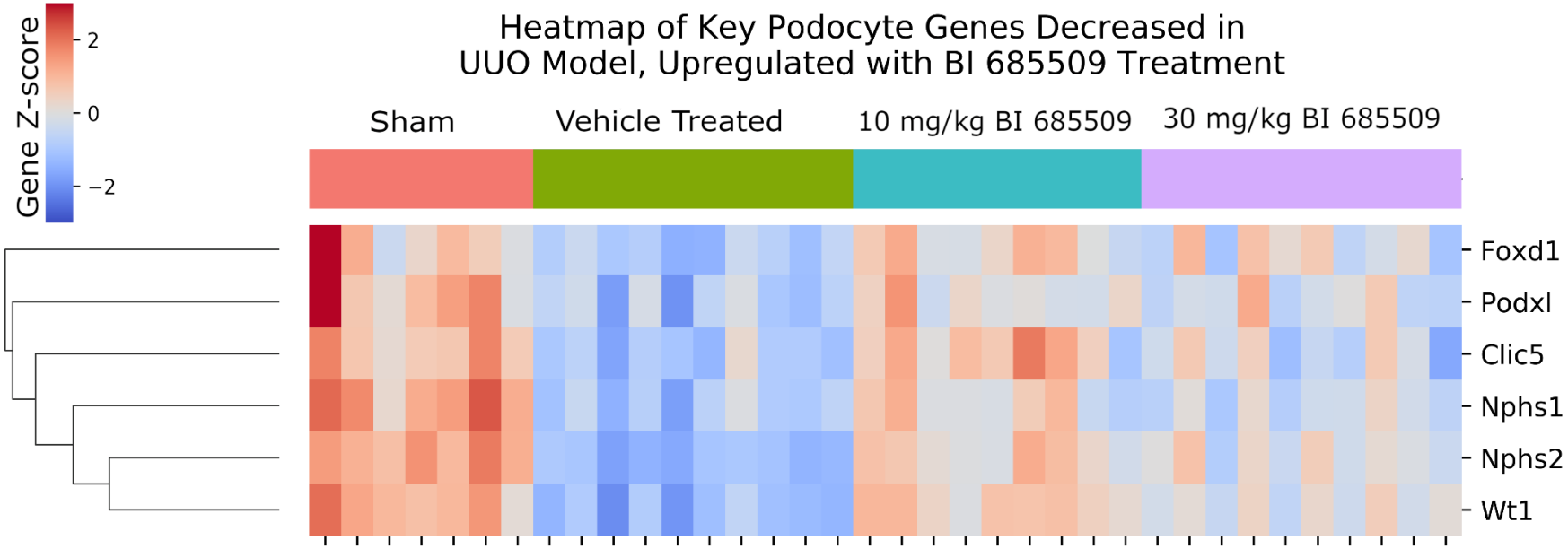

Supplemental Fig. 7. Heatmap of podocyte-associated genes decreased in UUO model and upregulated in groups treated with 10 mg/kg and 30 mg/kg doses of BI 685509.

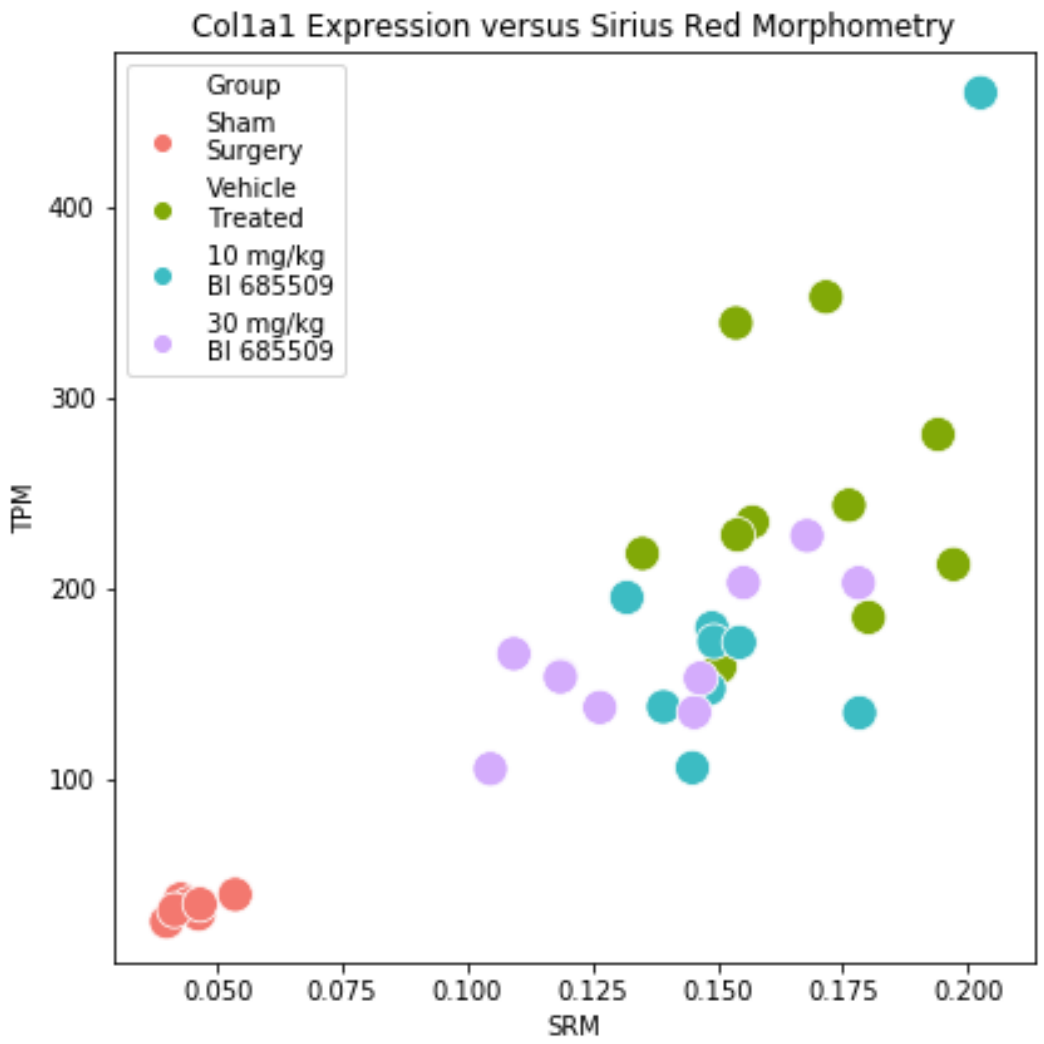

Supplemental Fig. 8. Scatterplot of the relationship between Col1a1 expression by RNAseq and Sirius Red Morphometry.